THE EFFECT OF HEAT TREATMENT ON THE ADIABATIC SHEAR BANDS IN AISI 4340 STEEL AT HIGH STRAIN RATE

By

Sahar Al-ameeri

A thesis
submitted to the faculty of graduate studies
in partial fulfillment of the
requirements for the degree of

MASTERS OF SCIENCE

Department of Mechanical and Manufacturing Engineering
University of Manitoba
Winnipeg, Manitoba

THE UNIVERSITY OF MANITOBA

FACULTY OF GRADUATE STUDIES

*****

COPYRIGHT PERMISSION

"The Effect of Heat Treatment on the Adiabatic Shear Bands in AISI 4340 Steel At High Strain Rate"

BY

Sahar Al-Ameeri

A Thesis/Practicum submitted to the Faculty of Graduate Studies of The University of Manitoba in partial fulfillment of the requirement of the degree

Of

MASTER OF SCIENCE

ABSTRACT

The presence of adiabatic shear bands (ASBs) in a material is detrimental to their structural integrity and may lead to unexpected failure in service. Most of the previous research work has been devoted to initiation and propagation of adiabatic shear bands. This research is focused on process reversal of adiabatic shearing with the ultimate intent of eliminating the deleterious effect of adiabatic shear bands in structural parts which has been subjected to high strain rates during forming or in service. The effect of heat treatment on structure and mechanical properties of (ASBs) is investigated in this study.

Two groups of AISI 4340 steel cylindrical samples were austenized, oil quenched and tempered at 315°C for 1 hr or 425°C for 1hr respectively, followed by air cooling. The two groups were impacted at high strain rates using the modified Split Hopkinson Pressure Bar (SHPB) to produce adiabatic shear bands in the steel samples. Microstructural evaluation and hardness tests were conducted on the specimens after the impact test. White etching ASBs were mostly observed in the impacted steel samples under the optical microscope. The hardness in the shear band region is much higher than in the rest of material. Since the objective of this research is to eliminate the effect of these bands, selected samples were heat treated at 315, 400, 500, 600 and 650 °C. The heat treatment time varied between 20 min and 2 hrs.

Heat treatment of the adiabatic shear bands at 315 °C for two hours did not produce any noticeable change in the structure and hardness of adiabatic shear bands in the impacted steel samples. As the tempering temperature was increased from 300 to 600°C for a soaking time of 1 hr, recovery of the pre-impact microstructure and properties in the shear bands became more pronounced. At 400 °C, no significant change occurred while the change became pronounced as the temperature was raised to 500 °C. However, heat treatment of the shear bands at 650°C for 20 min. showed a significant change in the microstructure. The hardness of shear bands also decreased considerably. Complete microstructure and property recovery in the adiabatic shear band was obtained by heating the impacted samples at 650°C for 2 hrs. The brittle white adiabatic shear bands are completely replaced with a ductile material whose microstructure is similar in appearance to the bulk material. A considerable change occurred in the shear bands by heat treating at 600 °C for 1 hr.

The results of this study showed that microstructural changes taking place during adiabatic shearing can be reversed by a heat treatment procedure. It is suggested that the associated microstructural and property changes can be traced to nucleation of new grains by coalescence of fine sub-grains in the adiabatic shear bands.

ACKNOWLEDGEMENTS

I would like to acknowledge the people, who contributed to a successful completion of this work. My appreciations go to my husband, my parents and my kids for their patience and support. I am very grateful to my supervisor, Professor M.N. Bassim for all his unflinching support, encouragement and guidance. His deep understanding of my personal situation is greatly valued and highly appreciated. I thank Dr. Akindele Odeshi for his guidance and endless support for a successful completion of this work. I am also grateful to Dr. Moses Owolabi for taking the time to review the final draft of this work. The assistance of Dr. Q. Li in the experimental work of this study is also is appreciated. My gratitude also goes to Dr. J.R. Cahoon and Dr. Norman Richards for their valuable course materials and for their time as committee members. To Dr. Ahmed Shalaby, my external examiner, I say big thank you for your time. I thank Dr. Don Smyth, the acting Dean of Faculty of Graduate studies and Ms. Cassandra Davidson also of the Faculty of Graduate studies for their understanding, support and help. I also wish to acknowledge Dr. Douglas Thomson for his assistance and support in my experimental work. Lastly, lots of thanks to all the department technicians, office support staff, other graduate students and friends for their support.

TABLE OF CONTENTS

LIST OF FIGURES

LIST OF TABLES

CHAPTER ONE: INTRODUCTION

Plastic deformation in metals at high strain-rates is characterized by strain localization in narrow bands whose width may be in the range of about 100 μm. The strain localization is usually caused by adiabatic heating in which heat generated during deformation is concentrated and conserved along a narrow band. The heat is not conducted away leading to a local rise in temperature. The thermal softening effect of the local rise in temperature will cause a mechanical instability leading to stress collapse and strain localization along the narrow band. These narrow bands are called adiabatic shear bands. They have been observed in metallic materials after rapid deformation. Adiabatic shear bands in metals are generally harder and more brittle than the parent material and can act as precursors to failure during dynamic loading. Many failures under dynamic loading have been traced to formation of adiabatic shear bands which subsequently crack and lead to materials' fragmentation. Material degradation due to formation of adiabatic shear bands can be found in ballistic impact, high speed machining, explosion fragmentation, metal forming processes among others.

Two types of adiabatic shear bands have been identified in the literature: deformed bands and transformed (also called white etching bands) bands. Deformed bands are similar in appearance to the bulk material but consist of highly distorted and elongated grains. They are commonly formed in some nonferrous alloys and in pearlitic low carbon steels. When observed under optical

microscope transformed bands appear as white bands whose microstructural features are difficult to be resolved using either optical or scanning electro microscope. The word "transformed" is used to describe this type of band because of the notion that the white color of the band is due to the austenization of the bands during adiabatic heating and subsequent transformation into untempered martensite on rapid quenching by the surrounding matrix. Results of several other investigations, as will be enumerated in the literature review, have however disproved this theory. The hardness of white etching bands has generally been found to be comparable to that of untempered martensite. A review of microstructure and properties of both types of adiabatic shear bands is provided in detail in chapter two of this thesis.

Formation of adiabatic shear bands in a material during deformation at high strain- rate can be regarded as a failure process even if fragmentation or fracture of the material has not occurred. Adiabatic shear bands will act as crack initiation sites during subsequent dynamic or quasi-static loading leading to premature and unexpected failure in service. The presence of adiabatic shear bands in a material will impair its mechanical integrity and is therefore not desirable in structural parts. Several previous investigations on adiabatic shear bands since 1944, when it was first reported, have been focused on its initiation and propagation both from material science and solid mechanics point of view. The present investigation is aimed at process reversal of adiabatic shearing. The objective is to explore the possibility of using heat treatment procedure to remove

adiabatic shear bands or to reduce the deleterious effects on the structure and mechanical integrity of engineering materials.

In order to achieve the set research objective, cylindrical samples machined from AISI 4340 steel were subjected to rapid deformation by direct impact using Split Hopkinson Pressure Bar (SHPB). The impacted samples were evaluated for adiabatic shear bands formation during impact loading and were subsequently subjected to annealing treatment at temperature between 300 and 650 °C to determine the effect of various heat treatment procedures on the structure and material properties of the adiabatic shear bands in the impacted samples. In addition, the effects of microstructure on the structure and material properties of adiabatic shear bands formed during impact were also studied. The failure mechanism of the adiabatic shear bands in samples that failed during testing was investigated and is discussed in this research study.

CHAPTER TWO: LITERATURE REVIEW

2.1 Summary

Plastic deformation of metals and alloys under quasi-static-loading and low strain rates at moderate strains is governed by slip and twinning mechanisms. Both slip as well as twin deformations depend mainly on the crystallography of the plastically deforming material. Deformations under quasi-static loading or low strain rates are relatively uniform across the cross section of the material. The mechanism of plastic deformation at high strain rates such as ballistic impact is a complex phenomenon that is dominated by strain localisation along narrow bands. Most sudden and unexpected failures of normally tough materials under impact loading have been traced to this strain localisation during deformation. Most of research studies to date are focused on mechanistic and microstructural evaluation of the adiabatic shear bands. To the best of my knowledge, there has been no intensive research on how to reverse the microstructural and property changes accompanying adiabatic shearing. A review of previous work on initiation, propagation and properties of adiabatic shear bands is presented in this chapter.

2.2 Adiabatic Shear Bands (ASBs)

Adiabatic shear bands (ASBs) are regions of extreme localized deformation in materials that are subjected to dynamic mechanical loading. During high strain-

rate deformation of a solid material, adiabatic heating may occur, whereby the heat generated during the deformation in a particular region is retained and not conducted away. This can cause a local rise in temperature and create a condition whereby the thermal softening effect of adiabatic heating is greater than the strain hardening effect of the deformation. Consequently thermo-mechanical instability occurs in the material, resulting ultimately in an extreme localization of deformation along narrow bands called adiabatic shear bands. In many cases this strain localization can cause material fracture. When fracture does not occur, the mechanical properties of a material will be impaired by the presence of shear bands. Adiabatic shear bands are usually more brittle than the bulk material and can serve as preferred path for crack initiation and propagation during subsequent loading. The phenomenon of adiabatic heating leading to strain localization and formation of shear bands during high strain-rate deformation was first described by Zener and Holloman in 1941 [1]. Numerous investigations have since been carried out to understand the mechanistic and metallurgical aspects of adiabatic shear bands. Although shear bands can be observed in a metal that is subjected to lower strain-rate deformations, the termed adiabatic shear bands is employed when the strain rate is greater than $10^2\ s^{-1}$ [2].

Shear bands formation has been observed in a wide range of pure metals and alloys including steels [3], ultra-fine-grained (UDG) iron [4], pure titanium [5], titanium alloys [6], tungsten alloys [7], aluminum alloys [8] copper [9], Nickel

alloys [10], tantalum alloys [11], metallic glasses [12], and metal matrix composites [13] among others. Shear bands formation have equally been reported in various applications involving rapid deformation. Such applications include high speed machining, ballistic impact, metal forming processes and explosion fragmentation [14-18]. An Investigation by Wright [19] showed that the average strain rate in the flow zone when machining a low carbon steel at 183 m/min and 0.5 mm/rev was 10^4 s^{-1}. This strain rate is sufficiently high enough to promote adiabatic heating and strain localization during the machining operation. This explains the formation of ASBs in the region closed to the machine surface of most metals after high speed machining.

Two major types of adiabatic shear bands have been observed in metallic materials in the literature. In quench and tempered steels, adiabatic shear bands appear as distinct white bands when observed under an optical microscope after etching. The white etching band is completely different in appearance from the surrounding bulk material. In pearlitic and ferritic steels and in most non ferrous metals, the shear bands appear as largely deformed narrow bands showing strong evidence of large shear distortion in that region during deformation. The white etching ASBs found in steel are sometimes referred to as transformed bands and are considered a product of transformation from austenite to untempered martensite. It was suggested that the structure in the narrow bands is converted to austenite during adiabatic heating while the austenite transforms to martensite through rapid quenching by the surrounding matrix [20].

Results of many research studies however disagree with the suggestion of austenite-to-martensite transformation during formation of the white etching ASBs found in steels. For example, Cho et al [21] measured temperature distribution in the shear bands of HY-100 steel during high strain rate deformation and reported maximum temperature to be about 600 °C. Duffy and Chi [22] also reported a maximum temperature of 600 °C in ASB during high strain deformation of HY-100 and AISI 4340 VAR steel. The fact that this maximum temperature is below the austenitization temperature raises some doubts on the possibility of austenite formation during adiabatic shearing. Where mathematical modeling of conversion of plastic deformation energy into heat suggests a temperature rise into the austenitic region, the soaking time at that temperature is insufficient for transformation into austenite to occur. Without austenitization of the shear band, martensitic transformation during adiabatic shearing cannot occur [23]. Several transmission electron microcopy studies on white etching bands in steels showed the shear band to consist of very fine grains of submicron size [15, 23, 25, and 26]. Zurek [26] suggested that the white nature of the etching (ASBs) in steels is due to the resolution limit of optical microscopy in resolving the nanometer substructure of the shear bands.

2.3 Initiation and Propagation of Adiabatic Shear Bands

2.3.1 Stages in plastic deformation at high strain rate

According to a study by Marchand and Duffy [27], plastic deformation of metallic materials appears to follow a three stage process which begins with a homogeneous strain state, followed by a generally inhomogeneous strain state and finally by a narrowing of localisation in to a fine shear band. A typical stress strain curve showing strain values at which each of the three stages of deformation occur, as recorded by Marchand and Duffy, is given in Fig. 2.1. Three still cameras were focused on a HY 100 steel sample undergoing torsional rapid deformation to provide simultaneous photographs at different locations on the sample's surface.

The first stage of deformation representing the stage of homogenous deformation was observed from initial yield to a strain of about 0.23. Inhomogeneous deformation stage was observed above the strain values of 0.27. As deformation proceeds at this stage, magnitude of localized strain increases and the width of the region over which localization occur, decreases. In the investigated steel samples, Marchand and Duffy reported that with an increase of nominal strain from 0.27 to 0.35, the localised strain increased from about 0.48 to 1.70 over a band width that is decreasing from 600 μm to 150 μm. The third stage marking the extreme localisation of strain to very narrow bands was recorded at nominal strain greater than 0.38. A strain of up to 1900 % was recorded at this stage.

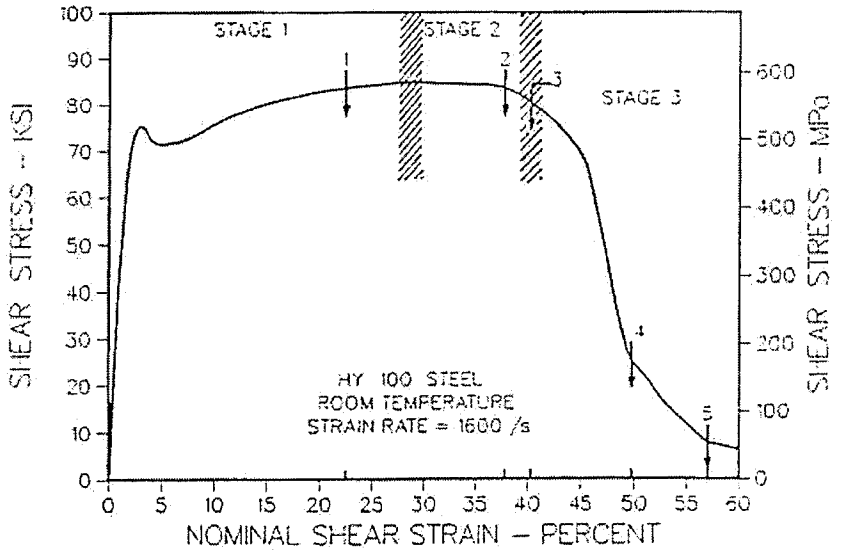

Fig. 2.1: Dynamic stress-strain curve showing three stages of deformation at high strain rate [27]

A relationship between the width of the shear band (w) and the strain within the shear band (γ_{LOC}) in HY 100 steel was deduced to be:

$$\gamma_{LOC} = a\, w^{b} \quad . \tag{2.1}$$

Where (a) and (b) are constants.

Many investigators have attributed the process by which deformation zone narrows to an extremely fine shear bands at the final stage during high strain-rate deformation to stress collapse as a result of the dominating thermal effect of softening in the shear band, thereby creating a state of thermo-mechanical instability [14, 27, 28, and 29]. Wright and Walter [28] investigated the dynamics of stress collapse leading to adiabatic shearing and inferred that the loss in strength has greater significance than the localization of strain. Schoenfeld and Wright [14] reported that stress collapse and strain localisation in a material undergoing rapid deformation occur at the most prominent non uniformity, which may occur due to specimen design, wave propagation or internal imperfections in material structure. Feng and Bassim [30] suggested that the presence of geometrical defects in material can improve the initiation of (ASBs).

Typical responses of a material undergoing plastic deformation are shown in Fig 2.2 [14]. Plastic deformation involves two simultaneously occurring effects: thermal softening as a result of the conversion of part of the deformation energy into heat energy and strain hardening due to dislocation multiplication effects of deformation, which effect predominates at any point in time depends on

deformation temperature and strain rate. For deformation at low strain rates or if adiabatic heating is suppressed, the strain hardening dominates the deformation process and the material may continuously become hardened at large strains indicated by the isothermal curve in Fig. 2.2. Plastic deformation at high strain rates will, however, produce adiabatic heating which leads to stress reduction with strain as a maximum flow stress is reached. Below the maximum flow stress, work hardening dominates the deformation process while thermal softening effect of adiabatic heating dominates beyond the maximum flow stress. For a perfect material with uniform distribution of stress, strain and temperature, softening may continue indefinitely [14]. However non uniformity in the material will lead to stress collapse, strain localisation and formation of ASBs.

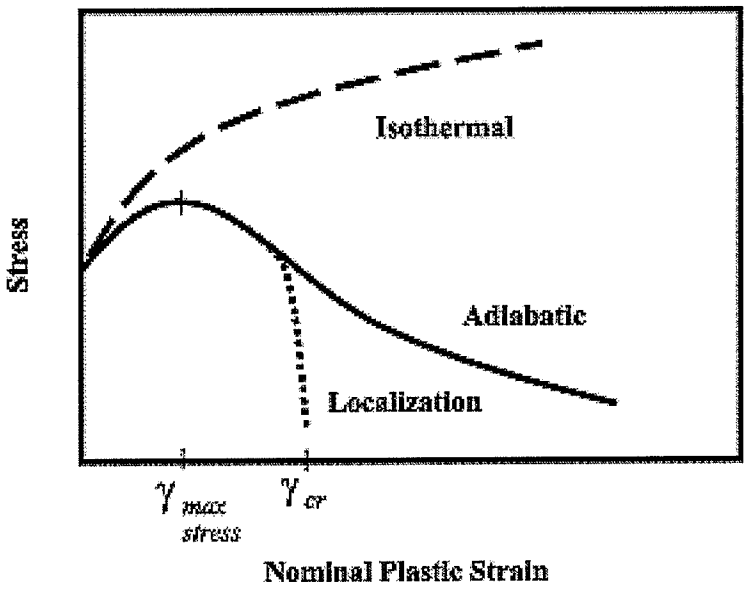

Fig. 2.2: Typical response of a work hardening material to plastic deformation

2.3.2 Initiation mechanisms

Four possible shear band initiation mechanisms have been indentified in single phase homogenous materials [31]. They are grain size inhomogeneity, geometrical softening, Peirce-Asaro-Needleman [30] textural localisation and dislocation pile-up release as schematically presented in Fig. 2.3. A larger grain which exhibits a lower yield than smaller grain may deform preferably and acts as shear band initiation site under dynamic loading. Geometrical softening can occur as a result of grain rotation leading to localised softening and initiation of shear bands. Localised deformation of a grain can result in extended strain-localised band through cooperative plastic deformation of grains as proposed by Pierce et al [32], Anand and Kalidindi [33], and reviewed by Nesterenko et al [31] (Fig. 2.3c). A local rise in temperature and softening can be produced when a dislocation pile pierces through a grain boundary creating a site for shear band initiation as proposed by Armstrong and Zerilli [34] and schematically presented in Fig. 2.3d by Nestrenko et al [31].

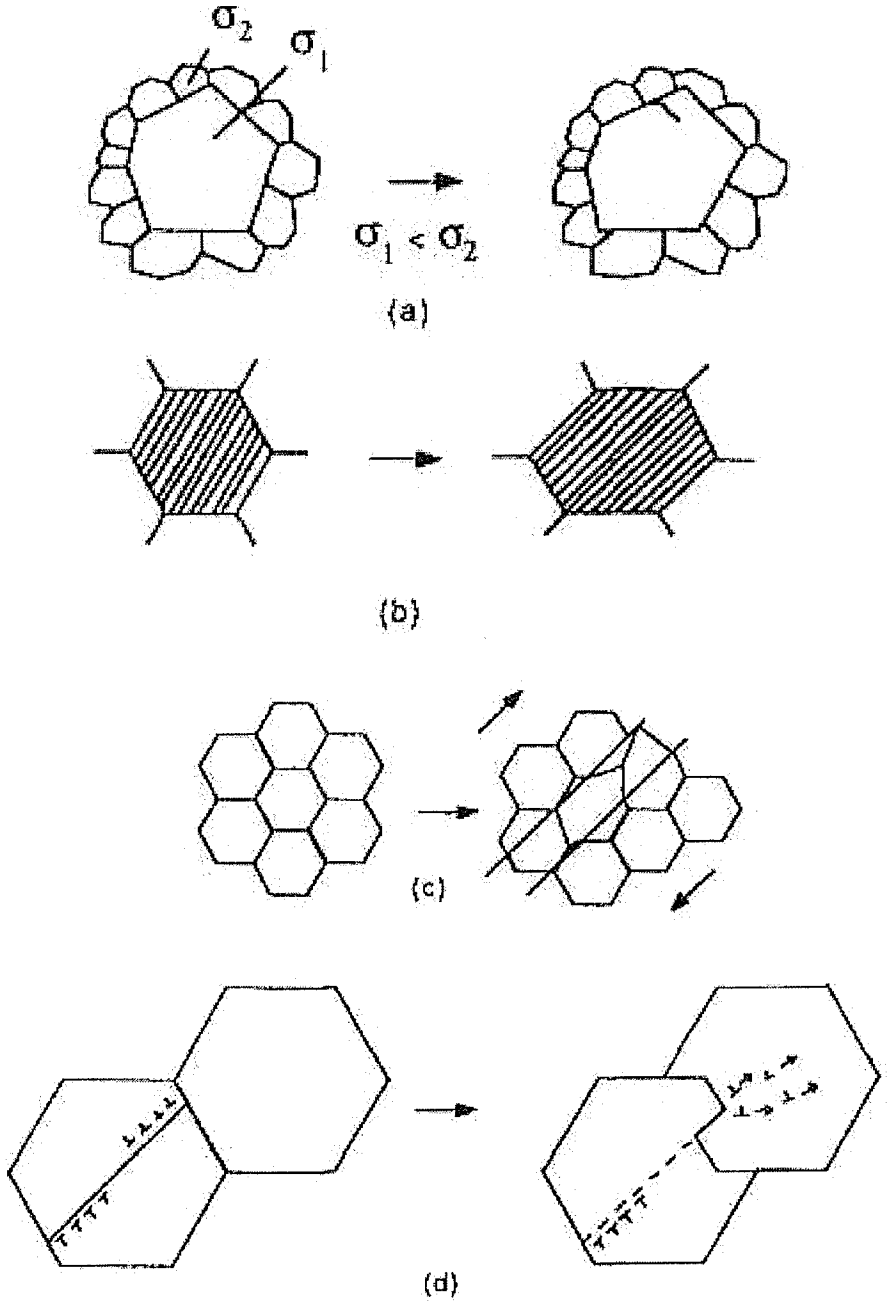

Fig. 2. 3 : Possible shear-band initiation mechanisms in single-phase homogeneous materials. (a) grain size inhomogeneity, (b) geometrical softening, (c) Peirce-Asaro-Neddleman textural localization and (d) dislocation pile-up release [30].

2.3.3 Constitutive relations

Several constitutive equations governing adiabatic shearing has been developed, some of which can be used to predict various boundary parameter governing adiabatic shear localisation. Johnson-Cook's model [35] was proposed for metals undergoing large deformation at high strain rates and high temperature. According to this model, the flow shear stress is given by the equation (2.2)

$$\tau = (A + B\gamma^{n})\left(1 + C\,In\frac{\dot{\gamma}}{\dot{\gamma}_{o}}\right)\left[1 - \left(\frac{T - T_{ref}}{T_{melt} - T_{ref}}\right)^{m}\right] \qquad (2.2)$$

Where A the static yield strength, B the strain hardening parameter, γ the equivalent plastic strain, n the strain hardening exponent, C the strain rate parameter, $\dot{\gamma}$ the equivalent plastic strain rate, γ_{o} the reference strain rate, T the temperature, T_{ref} the reference temperature, T_{melt} the melting temperature, and m the temperature exponent. Johnson Cook's model shows that the flow stress is a function of strain hardening coefficient, the strain-rate sensitivity and temperature. According to this model, the flow stress will drop to zero when the temperature in the shear band region reaches the melting temperature. The dynamic stress-strain curves have also been described by power law as given in equation (2.3) [36, 37]:

$$\tau = \tau_{o}\left(\frac{\gamma}{\gamma_{o}}\right)^{n}\left(\frac{\dot{\gamma}}{\dot{\gamma}_{o}}\right)^{m}\left(\frac{T}{T_{o}}\right)^{v} \qquad (2.3)$$

Where τ_o is the static yield stress, n is the strain hardening coefficient, m is the strain-rate sensitivity, v thermal softening coefficient, γ_o is the strain at yield in a quasi-static simple shear test, $\dot{\gamma}$ is the strain rate, $\dot{\gamma}_o$ is a reference shear rate and T is the reference temperature. Several other models indicating the influence of various variables on the dynamic propagation of adiabatic shear bands are described in the literature [28, 29, 36-39]. For example an analysis by Wright [39] shows that the speed of adiabatic shear band can be estimated from its physical properties and constitutive equations.

2.3.4 Propagation of adiabatic shear bands

A single shear band may initiate and propagate in a material under high strain-rate deformation leading to fracture of the material into two pieces. Multiple shear bands simultaneously can initiate and propagate leading to fragmentation into several pieces. Xue et al [40] studied multiple shear bands formation in stainless steels by means of thick wall cylinder technique and identified various parameters which could influence shear-band distribution as machining effect, shrink fitting effect and annealing effect. Study by Nestrenko et al [40, 41] shows that shear bands form during high strain rate collapse of a thick wall titanium cylinder undergo self reorganisation as they initiate and propagate. The shear bands were shown to arrange themselves in periodic and characteristic spacing. An analysis by Grady and Kipp [42], further simplified by Nesterenko et al [40, 41], the constitutive equation predicting the shear bands spacing (L) as follows:

$$L_{KP} = 2\left[\frac{\rho k C}{\gamma^3 a^3 \tau_o}\right]^{1/4} \quad . \tag{2.4}$$

Where k is thermal conductivity, ρ is density, C is thermal heat capacity, and $\dot{\gamma}$ is the applied shear strain-rate. The following relation was assumed between flow stress and temperature.

$$\tau = \tau_o\left[1 - a\,(T - T_o)\right] \tag{2.5}$$

τ_o is the strength at a reference temperature T_o and a is a softening parameter. Grady and Kipp [42] analysis is based on stress collapse mechanism while ignoring work hardening and strain-rate sensitivity. A similar analysis was carried out by Wright and Oekendon [43] on the basis of small perturbation leading to nucleation of ASBs. According the analysis of Wright and Oeckendon, shear band spacing (L_{WO}), where multiple shear bands are formed, is given by

$$L_{WO} = 2\pi\left(\frac{kCm^3\dot{\gamma}_o^m}{\dot{\gamma}^{3+m} a^2 \tau_o}\right) \tag{2.6}$$

Wright-Oeckendon's analysis was based on the following assumption that

$$\tau = \tau_o\left[1 - a(T - T_o)\right]\left(\frac{\dot{\gamma}}{\dot{\gamma}_o}\right)^m \tag{2.7}$$

where $\dot{\gamma}_o$ is a reference strain rate and m is the strain rate sensitivity. τ_o is the flow stress at the reference temperature T_o and strain rate $\dot{\gamma}_o$

2.4 Microstructure and Properties of Adiabatic Shear Bands

Adiabatic shear bands in pearlitic steels appear as highly deformed materials. Investigations by Meyers and Wittman [2] on high strain deformation of a low carbon (0.2 wt. % C) steel show that white shear bands are formed only in the steel samples with martensitic and bainitic structures. The shear bands in the pearlitic (annealed or normalized) appear as highly deformed material. The microstructure of a deformed band was shown to be very laminar consisting of alternate highly elongated layers of ferrite and pearlite (Fig. 2.4). In aus-quenched steel, both deformed and white etching bands were observed, an effect which was attributed to difference in shearing strain at various locations. Meyer and Wittman suggested that for brittle pearlite to have such a high amount of deformation as observed under the microscope, a large amount of fracturing of the cementite carbides must have occurred. A study by Zhang et al [44] on shear banding in quenched and tempered low alloy steels showed that tempering temperature has considerable influence on the type of shear bands that is formed. Whereas deformed bands formed in specimens tempered at high temperatures, white ASBs formed in specimen tempered at low or medium temperatures.

Investigation on fine-blanking of annealed SS 400 steel by Chen et al [16] shows that the deformed band is also made up of elongated grains. The elongated grains were observed to align parallel to the direction of applied shear stress.

Microstructural evolution during formation of adiabatic shear bands shown to occur in 3 stages as schematically presented in Fig. 2.5. The 3 steps involved in the evolution of microstructure in the shear bands are as follows:

1. Alignment and elongation of grains in shear direction.
2. Partitioning of elongated sub-grains by transverse cell walls under high hydrostatic pressure and shear stress.

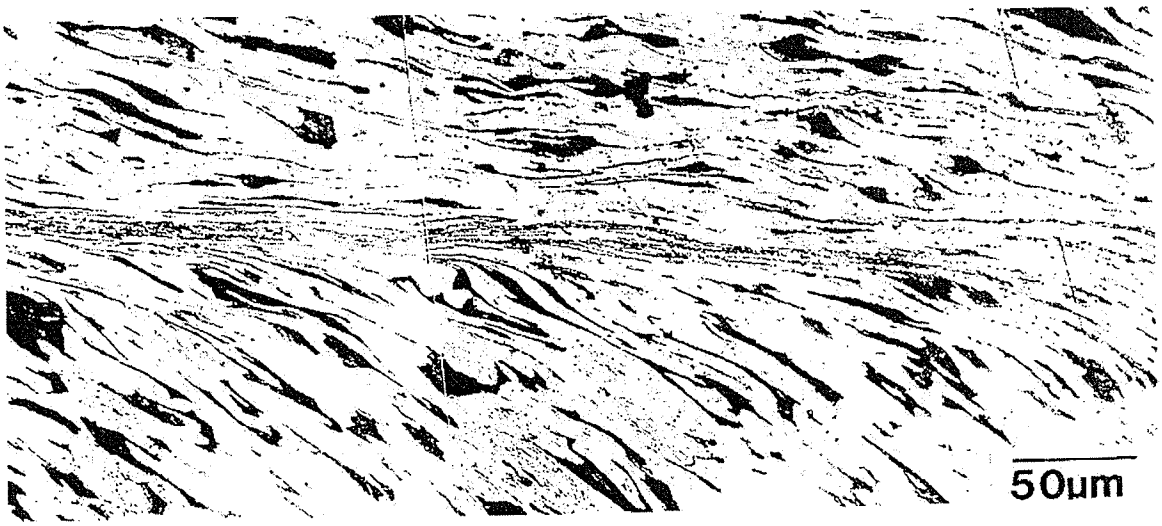

Fig. 2.4: Deformed band in a normalized AISI 1018 steel showing laminar structure consisting of layers of ferrite and pearlite [2]

3. Fragmentation of laminar and spheroidization of the cementite in the shear direction.

Fragmentation of cementite laminar in the deformation direction and partial spheroidization of cementite has also been reported by Zurek [26] during shear bands formation in pearlitic 4340 steel subjected to rapid deformation using a dynamic punch test. White ASBs was reported formed in this steel at average strain rate of 1800 s^{-1}. The size of the spheroidized cementite ranged between 0.1 and 0.05 μm and no evidence of martensite or phase transformation was observed in the shear band. An increase in hardness of about 30% was recorded inside the deformed band.

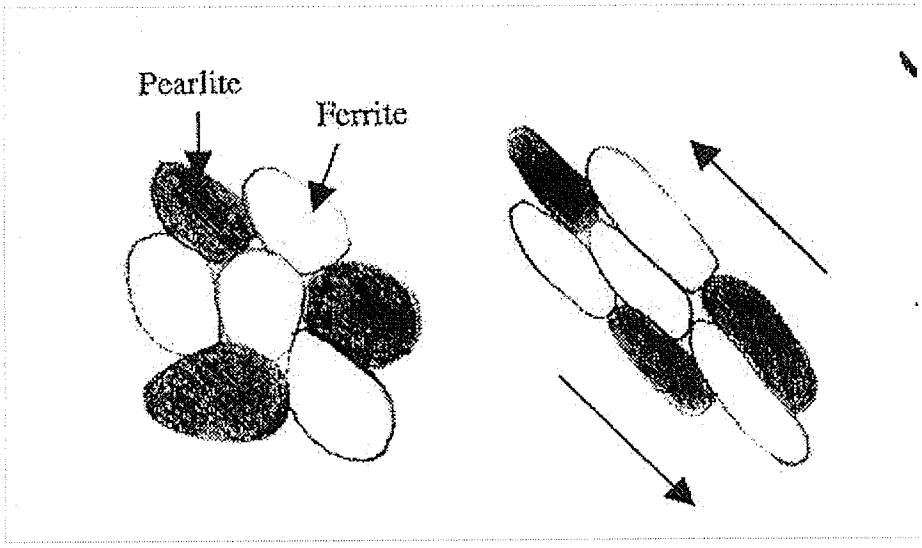

a. Original pearlitic structure

b. Reorientation and elongation of grains

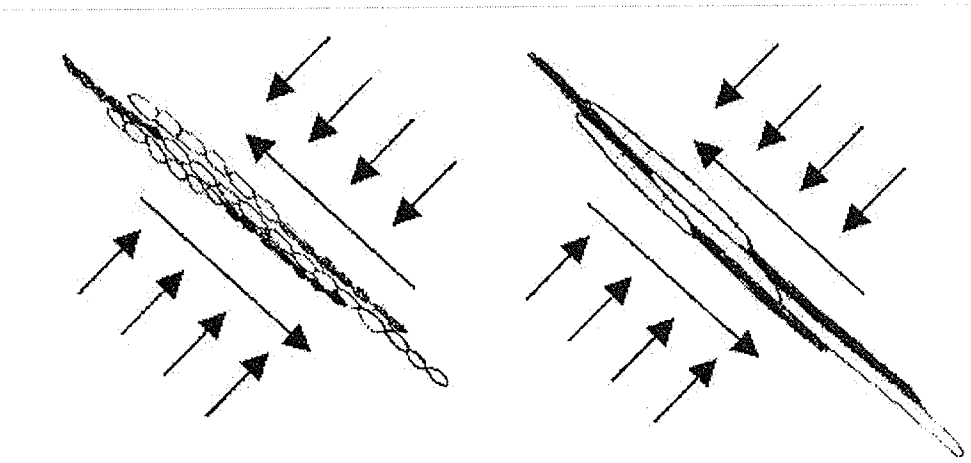

c. Cell wall formation on the elongated grains

d. Fragmentation of lamellae

Fig. 2.5: Schematic representation of the structural evolution during shear banding in fine-blanking process [16]

An investigation by Cho et al [21] on dynamic torsional deformation of HY-100 steel that was quench hardened and tempered at 638 °C indicates the formation of deformation band rather than white etching band during strain localization. TEM examination of the shear bands showed that microstructure of the shear band changed and showed no resemblance with the parent martensitic microstructure. The martensite laths were replaced by a more equiaxed structure within the shear band. The martensite laths were shown to bend and align in shear flow direction along the flanks of the shear bands. The aligned martensite laths along the flanks of the shear bands were found to be narrower than before. Cho and his colleagues observed two microstructures in the centre of the shear bands: (a) highly elongated narrow subgrains (laths) that extended in the shear direction, and (b) fine equiaxed cells with high dislocation densities. Schematic illustration of the microstructural evolution during adiabatic shearing as proposed by Cho et al is given in Fig. 2.6. Cho et al's findings agree with those of Zhang et al [44] that deformed bands are formed in quench hardened steels when they are tempered at high temperatures.

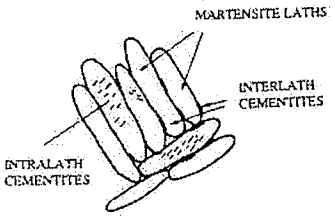

a. Undeformed structure(tempered Martensite)

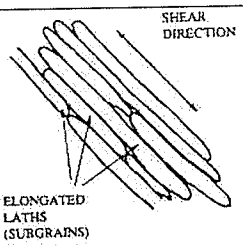

b. Reorientation and elongation of martensite laths in shear direction

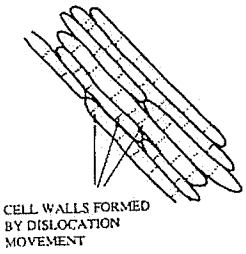

c. Partitioning of elongated subgrains into rectangular cells

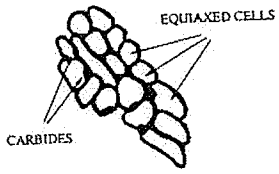

d. Formation of equiaxed cellular structure

Fig.2.6: Schematic representation of microstructural evolution during adiabatic shearing in HY-100 steel (quench hardened and tempered at 638°C [21].

Microstructural evaluation of white etching bands in martensitic steel by Wingrove [45] after high strain deformation shows the bands to consist of a high density dislocation and cell boundaries. The microstructure was not typical of normal martensite that is observed in steel but the diffraction pattern suggests that the microstructure consists of martensite. An investigation by Derep [25] on the structures of white etching bands in steels using transmission electron microscopy indicats that it consists of extremely fine martensite lathes and carbide grains at the outer region, while the centre of the shear bands consists of fine equiaxed grains of ferrite, iron carbides and austenite. The length and width of the martensite laths were found to be as small as 290 and 170 nm respectively. The mean carbide and ferrite sizes were measured to be about 30 and 135 nm respectively.

Studies by Meyers et al [24] shows that shear bands in stainless steels consist of two regions: one region comprises of extremely fine grains (0.1-0.2 μm) with well defined grain boundaries and a low density dislocations and another region having a glassy structure. The glassy region was formed by a solid state amorphitization process. TEM study of white layers produced in the surface of ball bearing steel by Liermann [46] shows that the white shear bands consist of very fine cells, less than 100 nm in size. Electron diffraction pattern showed that the band was composed of austenite and martensite in approximately equal parts. In addition, an amorphous region was also found in the white etching band region.

Barry and Byrne [15] conducted a TEM investigation on the surface white layer formed during machining of hardened steels and reported that the layer consists of very fine misoriented cells, with average size in the range of tens of nm. The microstructural feature of the cells could not be resolved reliably as a result of the extremely small size of the cells. They also reported that the structure of the white surface layer is different from that of conventional martensites found in steels. Increased amount of retained austenite in white etching bands have also been reported two other studies prompting the suggestion of reverse martensite transformation during formation of white ASBs in steels [25, 47]. In most cases, the conclusion of increased austenite in the shear bands were made based on observed FCC reflections in diffraction pattern of white etching bands and there has been no clear explanation on what can be responsible for increased retained austenite in the white etching bands formed in steels during rapid deformation. Barry and Byrne [15] suggested that retention of austenite is favored by the extremely fine size of the cells and the high dislocation densities around which Cottrell atmosphere may form and impede austenite transformation, Thus, while some authors like Glenn and Leslie [20] proposed martensitic transformation during formation of white etching bands, Barry and Byrne [15], suggested reverse martensite transformation. However, as discussed earlier, results of several other investigations [21, 22, 23, and 26] discuss the likelihood of any transformation taking place during formation of white shear bands and attribute the white color

of the shear bands to the limit of optical microscopy in resolving the nanosacled structure of white ASBs.

Shear bands are generally harder and more brittle than the bulk material. Investigations by Meyers and Wittman [2] showed that microhardness of shear bands in low carbon steels is independent of impact velocity. Microhardness transverses of bands in quenched 8620 steels were found to the almost identical for both tempered and aus-quenched structures, while the matrix microstructure hardness varied significantly. Rogers and Shastry [48] observe that the hardness of shear bands in steels is a function of carbon content. The increased in hardness in deformed bands can be attributed to work hardening in the shear localized region. In case of white etching bands, it may be due to work hardening as well as to structural changes that occur in the shear bands. Results of several investigations showed that the structure of white shear bands in steel consist of the same body tetragonal structure as the matrix, but with the carbide plates and martensite laths broken down by plastic deformation. Consequently the carbide plates and martensite laths will be replaced by a very fine microcrystalline structure [2, 23, 49].

Dynamic recrystallization in addition to dynamic recovery has been reported in adiabatic shear bands during strain localization in many metals [4, 11]. Unlike in static loading condition where the phenomena of grain recrystallization and growth are well studied and understood, recrystallization at high strain rates are

not so well understood or reported in the literature. The temperature rise and/ or time associated with adiabatic shearing are considered insufficient, in many cases, to achieve dynamic recrystallization and the kinetics of classical recrystalization models cannot account for the observed recrystallization behavior in adiabatic shear bands in many metals. A model of progressive sub-grain disorientation recrystallization has been proposed by Hines et al [11, 50]. This model is based on mechanically assisted sub grain rotation that is kinetically feasible in the stringent time and temperature profile of adiabatic shear bands in certain metals. It shows that the recrystallized grains present in the shear bands are the result of rotation of the recovered microstructure itself, with subsequent dislocation annihilation responsible for transformation of sub-grain dislocation walls to grain boundaries [9, 11, and 50].

The study on adiabatic shear bands on stainless steels using Electron Backscattered Diffraction (EBSD) by Meyers et al [24] also showed grain subdivision in the regions adjacent to adiabatic shear bands, with angular rotation in the scale of one grain (30 μm) of up to 20°. It was suggested that these rotations are due to the need to accommodate the imposed shear strain as well as to achieve compatible deformation between neighboring grains. Inside the shear band, the microstructure breaks down into units smaller than the resolution limit of EBSD method.

2.5 Factors influencing formation of Adiabatic Shear Bands

The susceptibility of a material to strain localization and subsequent adiabatic shearing depends on factors such as loading condition, heat capacity, heat conductivity, strength level, microstructure, geometry, defects and strain rate among others [44, 51, 52] . Adiabatic shear bands form readily in materials with low-strain hardening coefficient, low strain-rate sensitivity, low thermal conductivity, high thermal softening and high strength/hardness value [26, 52]. Lindholm et al [53] and Shrivastava et al [54] reported that formation of adiabatic shear bands in a material is strongly dependent on strain-hardening capacity of the material and the loading conditions. Zurek [26] submitted that ASBs are usually not formed under tensile loading because early void or crack growth during tensile loading prevents sufficient localisation of deformation. However during dynamic punch test which can typify a pure shear stress, Zurek observed that fracture by either void or crack formation was suppressed and local heating can accumulate to produce ASBs.

Microstructure plays a significant role in the formation of ASBs in metals. For example, investigations by Nakkalil et al [55] on high strain rate deformation of pearlitic steels show that the strain level for the onset of strain localization decreases with decreasing inter-laminar spacing of the pearlite. Zhang et al [44] conclude from their investigations on shear banding during ballistic impact that tempered martensite produces ASBs more easily than austenitic structures. The presence of abrasive particles was reported to favour occurrence of adiabatic

shear bands in impact wear. The presence of defects, imperfections and inhomogeneities in structure has severally been reported to promote adiabatic shear bands formation. Schonefeld and Wright [14] concluded that shear strain localization will occur eventually at the most prominent non-uniformity in structure. Feng and Bassim [30] observed that ASB cannot propagate without the presence of material or geometrical defects. Molinari and Clifton [56], Wright [57], Duffy and Chi [22] reported that the strain at which critical strain collapses occurs increases with increasing size of initial perturbations.

A study by Li et al [7] on adiabatic shear instability in tungsten alloys shows that specimen geometry has significant influence on its shear bands sensibility. While adiabatic shear bands did not form in the cylindrical specimens of the alloy, initiation and propagation of shear localization sequential to failure was observed in specimens having the geometry of a truncated cone. This result was attributed to uneven stress distribution in the truncated cone specimen. Bassim [58] studied the effect of specimen geometry in dynamic torsion test and observed that the dimensions of the test specimens influence the deformation process.

Bonnet-Lebouvier [38] studied the relationship between shear band propagation speed (C) and the loading condition that is typified by applied impact velocity (V) and showed that there exists a threshold velocity below which no shear band propagation is obtained as shown in Fig. 2.7. In addition three stages are noticeable: In stage I, C has an almost linear relationship with V. The relationship

tends to be nearly asymptotic in Stage II, while C only slightly increases with V in stage III. A dimensional analysis by Bonnet-Lebouvier et al [38] shows that in stage I, shear band propagation speed C speed is correlated to (a) material parameters: elastic modulus (μ), mass density (ρ) specific heat (C), heat conductivity (k), strain hardening coefficient (n) , strain rate sensitivity (m), Taylor-Quinney coefficient (β), stress level (K) and (b) loading conditions: applied velocity (V) and initial temperature (T_o) as follows:

$$\frac{C}{V} = \alpha \frac{K\beta}{\rho C_p T_0 m}\left(-An + B\right) . \qquad (2.8)$$

Where (A) and (B) are constants. This analysis shows that shear speed depends, in stage I, on stress level K and is independent of elastic modulus (μ). Increasing C_p will lead to decrease in shear band speed. A lower initial temperature (T_o) leads to increase in initial stress, to a stronger thermal softening and ultimately to increase in C. Increasing m and n will have a stabilizing effect on shear band and lead to reduction in shear band speed. Although the presence of initial geometrical defect is necessary for the initiation of adiabatic shear bands, Bonnet-Lebourvier [38] analyses suggest that shear propagation speed is independent of geometrical defects. Whereas it was difficult to obtain a simple relationship for stage II, Lebourvier et al obtained the following relationship for stage III:

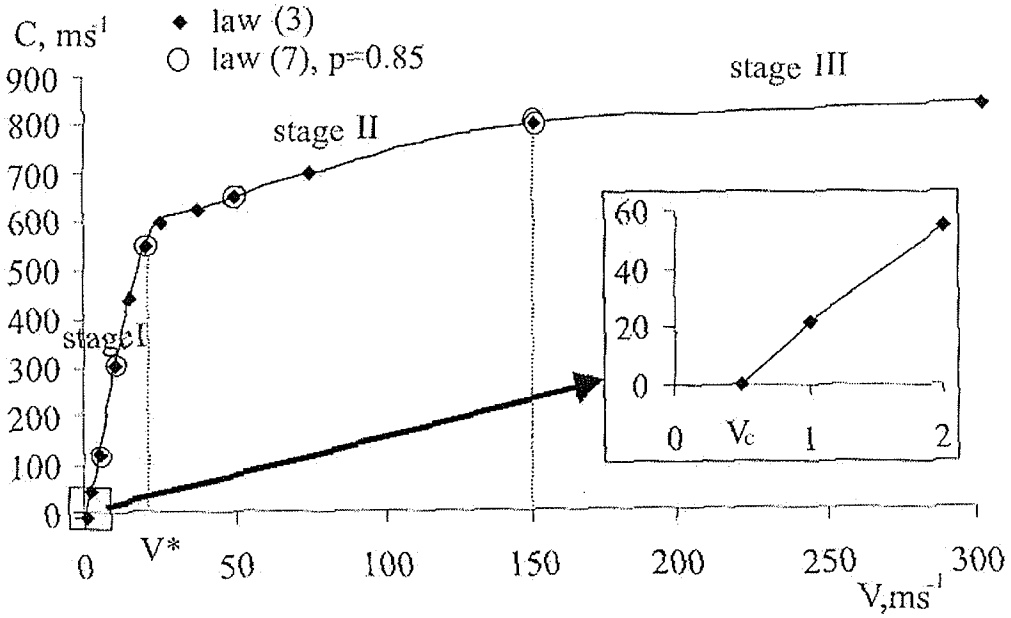

Fig. 2.7: Effect of applied velocity on the stationary shear band speed [38].

$$C = \eta C_2 \sqrt{\frac{K^2 \beta}{\mu \rho C_p T_0 m}} \left(-A'n + B'\right) \qquad (2.9)$$

This analysis shows that shear band speed propagation does not depend on V in stage III implying that external work does not influence the shear band propagation speed. Increasing the stress limit K leads to increased shear band speed in stage III as in stage I. The influence of thermal effects and parameters m, n, and k is the same as in stage I. The combined opposite effect of increased elastic modulus (μ) in increasing energy flux to the band tip (leading to an increase of C) and reducing the level of stored energy in front of band tip (producing a decrease of C) cancels the effects of elastic modulus on shear band speed [38].

2.6 Adiabatic shear bands failure

As described in the preceding sections, initiation of adiabatic shear bands during high strain rate deformation of a material is promoted by inhomogeneities in the material. Adiabatic shear bands can serve as precursors and preferential sites for failure, either by ductile void nucleation, growth and coalescence, or by cracking. It is suggested that high temperature of the shear bands regions make them to have lower flow stress than the surrounding matrix thereby generating tensile stresses which will open up voids in the shear bands [23, 59]. The level of damage accumulation, which leads to fracture, will depend on the magnitude of tensile stress across the shear band [26].

Xue et al [41] studied damage evolution within shear bands in Ti-6Al-4V alloy and reported that void evolution is comprised of the three main stages; nucleation, growth and coalescence as presented in Fig. 2.8. The voids, once initiated, will grow continuously into the surrounding soft matrix. According to the investigations by Xu et al, most voids first grow to the width of the band and then are elongated to elliptical shape along the direction of shear band. The second stage of void growth is characterised by the void elongation and rotation along direction of shear moment. At the third and final stage, the voids coalescence and generate cracks. A schematic representation of void nucleation, growth and coalescence resulting ultimately in cracks is presented in Fig. 2.9. If there are shear strains present concurrently with the tensile stress creating the voids, the voids are elongated and rotated as in Fig. 2.9b [41]. The final stage of crack elongation and rotation before failure is shown by the optical micrograph in Fig. 2.10.

The study by Erlich et al [61] showed that the absence of tensile stresses after impact resulted in bands with no voids, giving credence to the conclusion that tensile stresses open up voids in shear bands. Rogers [62] suggested two possible explanations for formation of voids in shear bands: (a) tensile stresses and (b) growth by cavitations within a heated zone during deformation. Atomic mobility at high temperature is responsible for formation of spherical voids to reduce surface energy [61, 63]. SEM Investigation of fracture surface of a

specimen that failed by shear band propagation by Guduru et al [64] showed elongated structure with sheared edges as in Fig. 2.11. This observation leads to the conclusion that the development of triaxial stresses in the shear bands produces void growth and ultimately leads to failure.

The increased hardness that is usually observed in shear bands makes them more brittle than the surrounding matrix and more susceptible to cracking. Investigations by Meyers and Wittman [2] on failure of quenched and tempered AISI 8620 steels subjected to ballistic impact show that shear bands precede cracking and in many cases cracks are intersected by other shear bands. A generalized schematic representation of damage of impacted steel targets is shown in Fig. 2.12. Spalling was found to occur in most cases at approximately 2 mm from the rear surface of the targets due to reflection of the shock wave at the free surface. Grebe et al [63] also reported two fracture modes in Titanium alloy plates subjected to ballistic impact (a) spalling induced by tensile pulses generated by the reflection of the shock wave at the back surface of the target and (b) shear tensile failures along shear bands. The characteristic dimpled appearance of the spalled surface is shown in Fig. 2.13.

Wright and Walter [28] suggested that the formation of adiabatic shear bands during high strain rate deformation results in reduction of shearing forces that can be transmitted through the material and cause failure. Li et al [12] report that the highly localized shear strain in the main shear bands in metallic glasses

generates a stress concentration, which can initiate a mode II shear microcrack. The mode II cracks will open and become shallow I + II complex cracks with the depth of 10 - 20 μm. It was observed that the test specimens fracture as soon as the complex crack became mode I crack, which propagate from the surface toward the centre.

In a review paper on failure dynamics, Klepaczko [65] suggested that one of the most possible hypotheses in exploring the failure criteria for adiabatic shear banding is that the maximum shear strain governs failure in ASB core. An instability strain $(\dot{\Gamma}_m)$ must be attained for catastrophic strain localization and failure to occur. Failure is assumed to occur when the plastic shear strain is α times larger than the instability strain, leading to the following failure criterion defining failure strain $(\dot{\Gamma}_C)$ in the core of ASB.

$$\Gamma_C(\dot{\Gamma}) = \alpha\Gamma_m(\dot{\Gamma}) \tag{2.10}$$

Where $(\dot{\Gamma})$ is the plastic shear strain rate. Another failure criterion for ASB considered by Klepacko in his article applied the hypotheses that strain energy density inside the ASB governs the failure. In this case the failure criterion defining the critical strain energy density for failure is given by

$$W_C(\dot{\Gamma}) = \eta W_m(\dot{\Gamma}) . \tag{2.11}$$

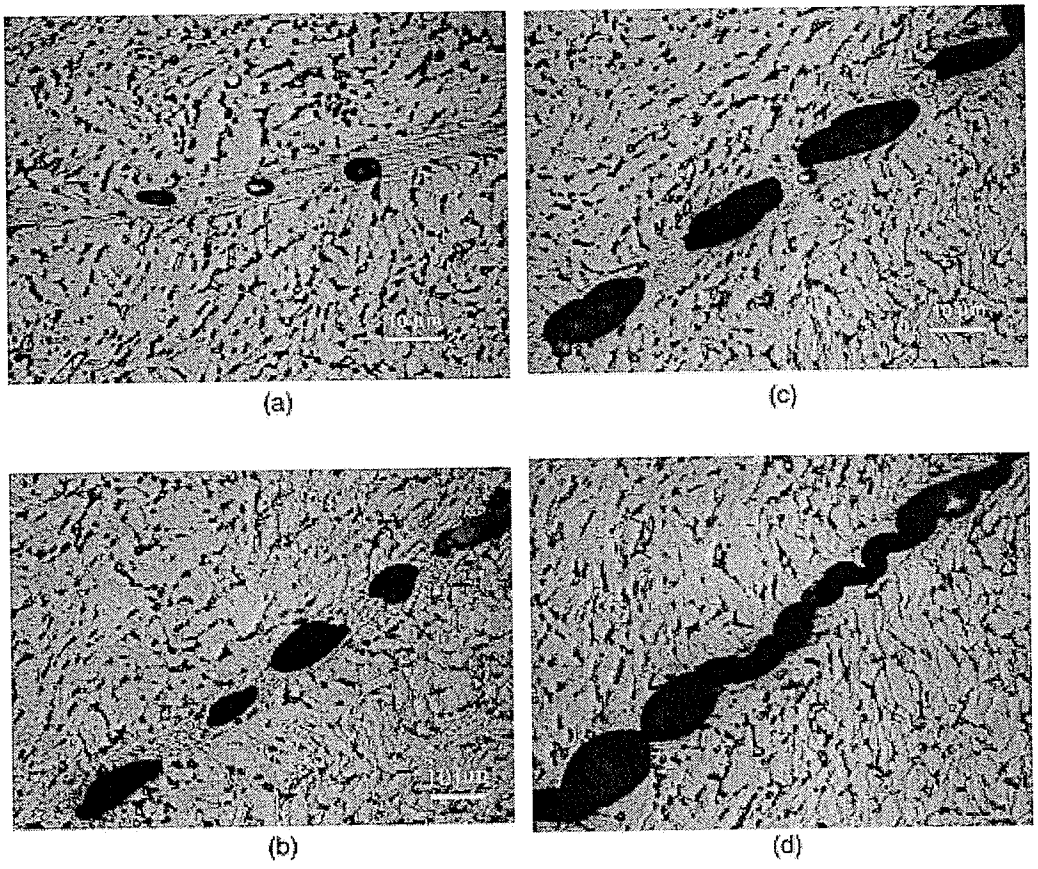

Fig. 2.8: Void nucleation and growth inside a shear band in Ti-6Al-4V alloy (a) nucleation of voids within a shear band, (b) growth of voids (c) elongation and rotation of voids (d) coalescence of voids to form crack [41]

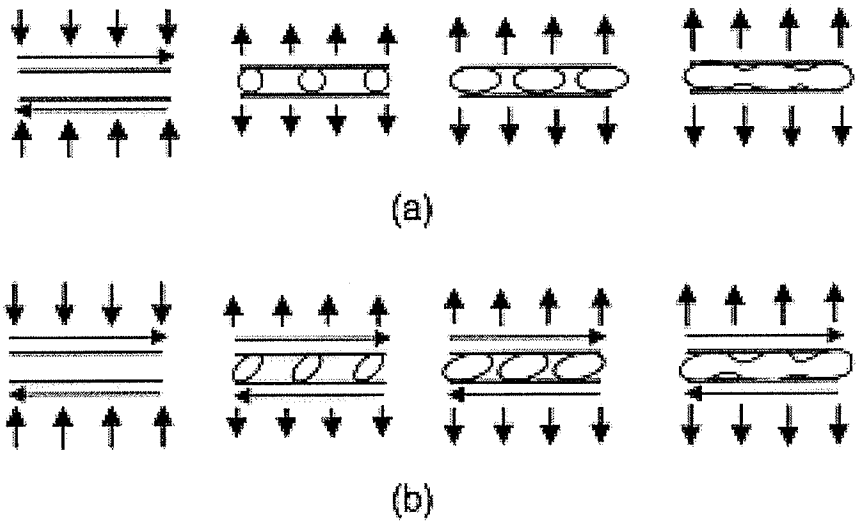

Fig. 2.9: Schematic representation of void nucleation, growth and coalescence in (a) absence and (b) presence of continuing shear [41].

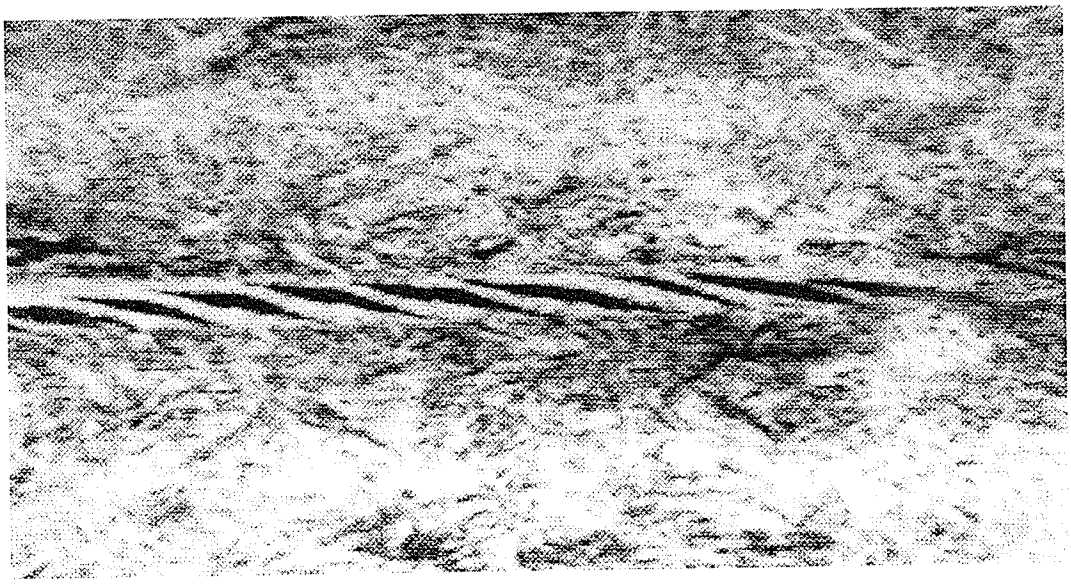

Fig. 2.10: The final stage of void elongation and rotation before failure [59].

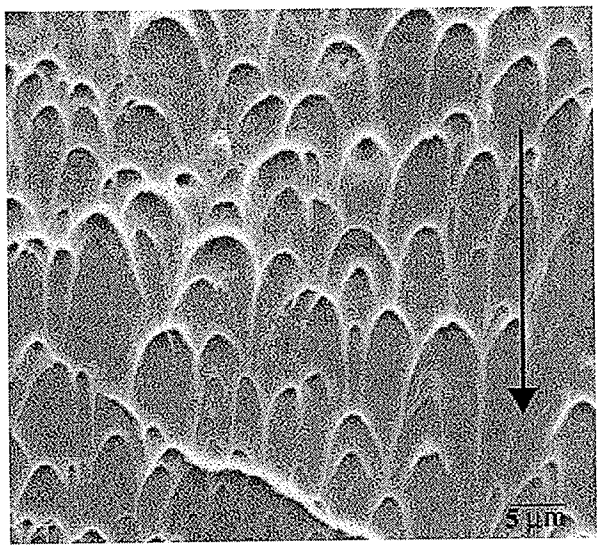

Fig. 2.11: An SEM image of the fracture surface that failed by shear banding. Arrow shows the crack propagation direction [64]

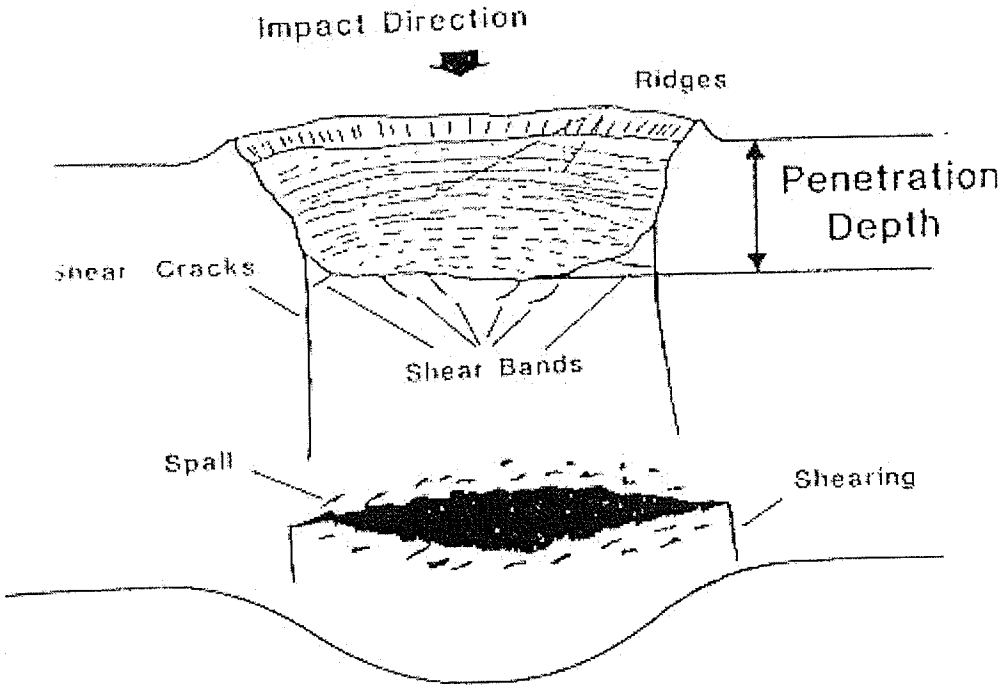

Fig. 2.12: Generalized schematic of expected damage on targets after ballistic impact [2]

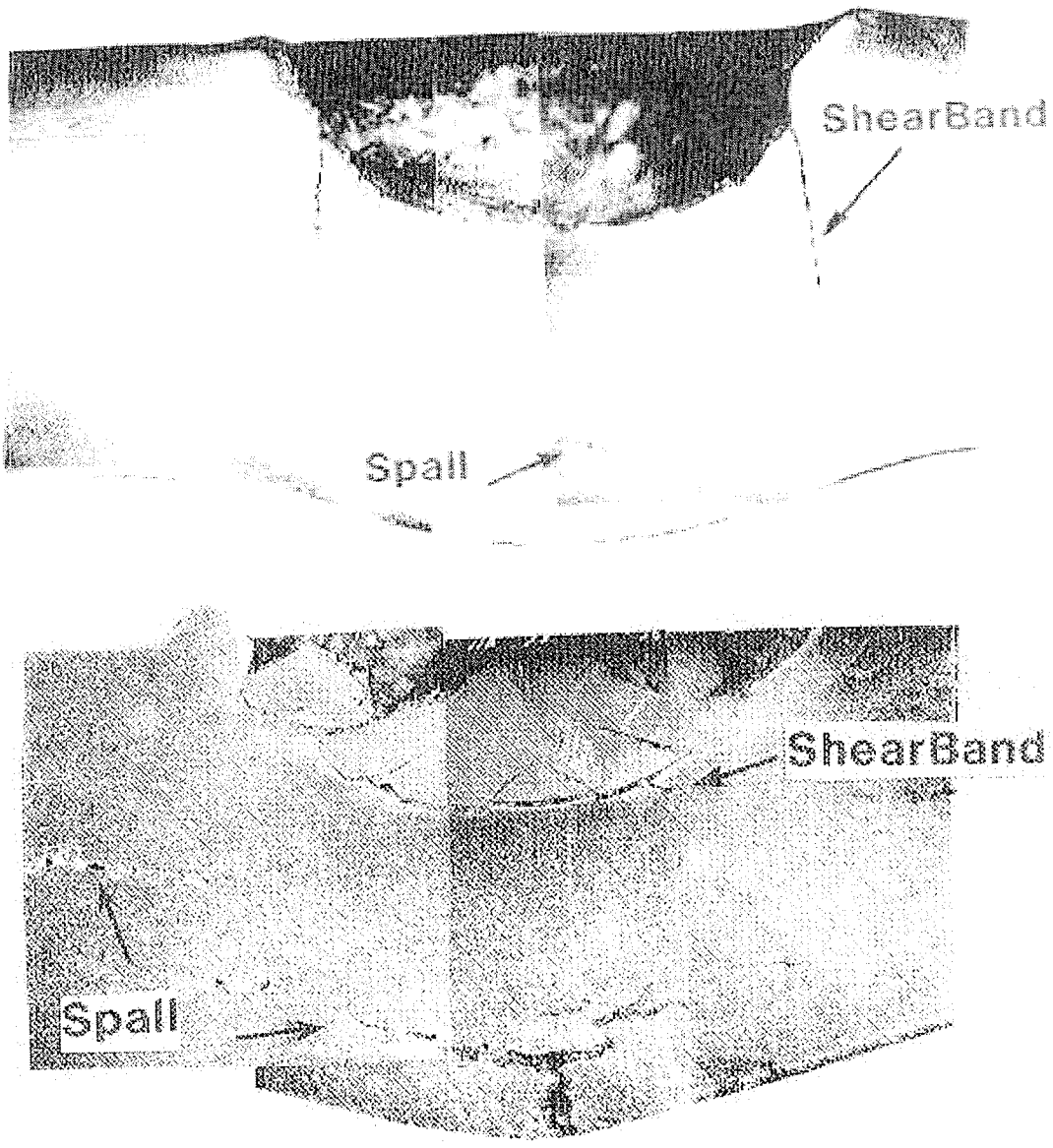

Fig. 2.13: Photomicrograph showing shear banding, spalling and cracking in steel targets after ballistic impact [2].

CHAPTER 3: EXPERIMENTAL PROCEDURE

3.1 Summary

Eighty cylindrical samples were machined out of rolled AISI 4340 steel bar. Samples were austenitized at 843°C for 30 minutes then quenched in oil. Half of the austenitized samples were tempered at 315°C for 1 hr. followed by air cooling, while the rest were tempered at 425 °C for 1 hr. and air cooled. The samples were subjected to rapid deformation by direct impact using Split Hopkinson Pressures Bar (SHPB).

The impacted samples were cut, ground, polished, etched and examined under optical and scanning electron microscopes to investigate the formation of adiabatic shear bands during impact. Both transverse and longitudinal sections of some samples were examined in order to picture the geometry of the shear bands in the impacted samples. As the objective of this research is to study the effective of heat treatment on the microstructure and the properties of the adiabatic shear bands in the metal, selected samples from each group after impact were heat treated at different temperatures to observe the changes in microstructure and micro hardness of the shear bands relative to the bulk matrix regions.

3.2 Material

The material used in this study is AISI 4340 steel. The chemical analysis of the AISI 4340 steel is presented in Table 3.1. The geometry of the test pieces is as shown in Fig. 3.1.

3.3 Heat Treatment of specimens before impact

All samples were austenitized at 843°C for 30 minutes followed by oil quenching to obtain a fully martensitic microstructure. Martensites have needle like structures and are generally very strong and hard, but brittle. The high strength and hardness of martensite is due to effectiveness of supersaturated interstitial carbon atoms in the body centre tetragonal structure of martensite in hindering dislocation motion. Moreover, there are few slip systems, along which dislocation movement can occur, in body centre tetragonal crystal structure. As-quench martensites are generally too brittle for any engineering application and must be tempered to improve the ductility and toughness. Tempering reduces internal stresses introduced into the steel during rapid quenching. Heated samples were divided into two groups; the first group was tempered at 315°C for one hour followed by air cooling, while the second group was tempered at 425°C for one hour and air cooled. Typical optical micrograph showing martensitic structure of the samples before impact is shown in Fig. 3.2.

Table 3.1: Chemical Composition of 4340 steel

Element	Compositions Wt %
C	0.38- 0.43
Mn	0.60- 0.80
P Max.	0.035
S Max.	0.040
Si	0.15- 0.35
Cr	0.70- 0.90
Mo	0.20- 0.30
Ni	1.65- 2.00

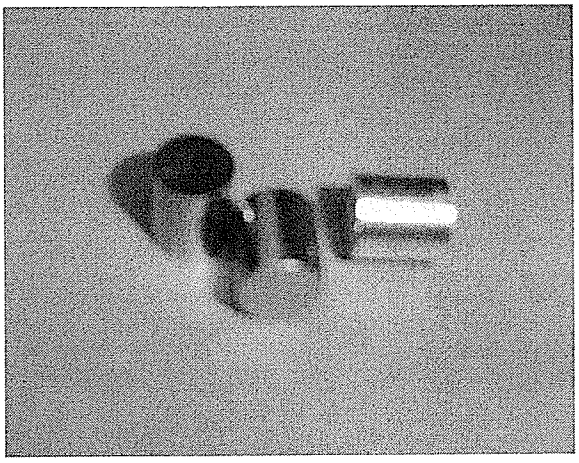

Fig 3.1: Cylindrical samples for impact test.

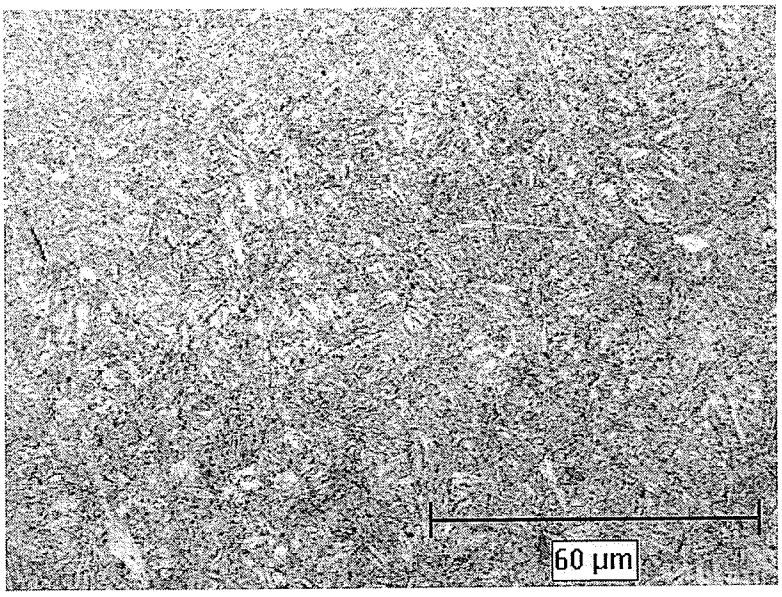

Fig. 3.2: Photomicrograph showing martensitic structure of the steel samples before impact

3.4 Impact Test

The two groups of the investigated samples were impacted using the modified Split Hopkinson Pressure Bar (SHPB). The firing pressure ranged between 100 and 250 KPa. All impact tests were conducted at room temperature and pressure.

3.4.1 Modified Split Hopkinson Pressure Bar (SHPB)

The Split Hopkinson Pressure Bar is the most commonly used method to investigate the effect of the high strain rate on different kind of materials. The SHPB which was developed from Bertram Hopkinson bar by Kolsky in 1949 [16] remains the standard equipment for measuring the response of engineering materials to high strain-rate deformation. Fig 3.3 shows a three dimensional view of the(SHPB). (SHPB) can produce higher strain rates (> 10^3 s^{-1}) than most other methods that have been developed for obtaining dynamic stress-strain curves for dynamic mechanical loading under tensile, compressive and torsional loading [17]. This apparatus consists of the following parts shows in (Fig. 3.4)

a. Accumulator and Firing Chamber

The compressed air in the accumulator is used to produce the pressure in the fire barrel to force the projectile to strike the sample at high strain rates.

Pressure gage is attached to the accumulator to measure the firing pressure

b. Control Box

This unit controls all the various parts of the SHPB and consists of the following parts:

- Power Switch button.
- Retract Reset button, which serves to bring the projectile to the start point.
- Charge button for initiating the charging process before firing.
- Accumulator Pressure button for controlling the firing pressure.
- Fire button for firing the projectile once the desired pressure has been attained.
- And the Pressure Gauge.

c. Gun Barrel

A hollow cylinder connected to the fire barrel to guide the projectile (4340 steel solid cylinder) towards the sample at high strain rate.

d. The Timer

Two sets of light beams are connected at 250 mm apart from each other. With this arrangement, the time for the projectile to travel a distance of 250 mm can be measured. The projectile velocity was calculated using this information.

e. Transmitter

The front face of the transmitter bar is used to hang the specimens using a high viscosity gel to keep it stuck to the centre of the bar. The transmitting bar is connected to a strain gauge and pulse amplifier which captures the transmitting elastic waves generated during impact and amplifies it before sending it to an oscilloscope. The oscilloscope captures and stores the strain wave's data in form of voltage time data. The data from the oscilloscope was analyzed with a computer process to obtain stress-strain data for the impact test. The transmitter bar is supported by wooden blocks to reduce the vibration. A wooden box is fixed around the sample to control the noise and to reduce the risk of flying parts in case of broken samples.

f. The Projectile

The projectile is a solid cylinder machined out of 4340 steel rod to the length and diameter of 127 and 38 mm respectively; the hardness of this cylinder after heat treatment was 47-HRC.

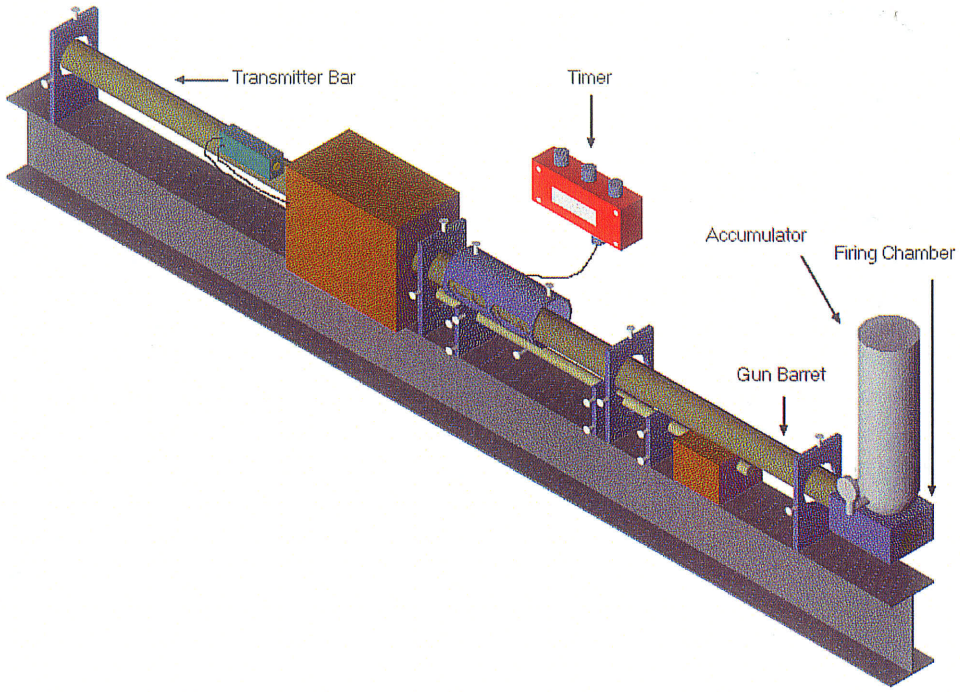

Fig. 3.3 Three dimensional view of the Applied Split Hopkinson Pressure Bar (SHPB).

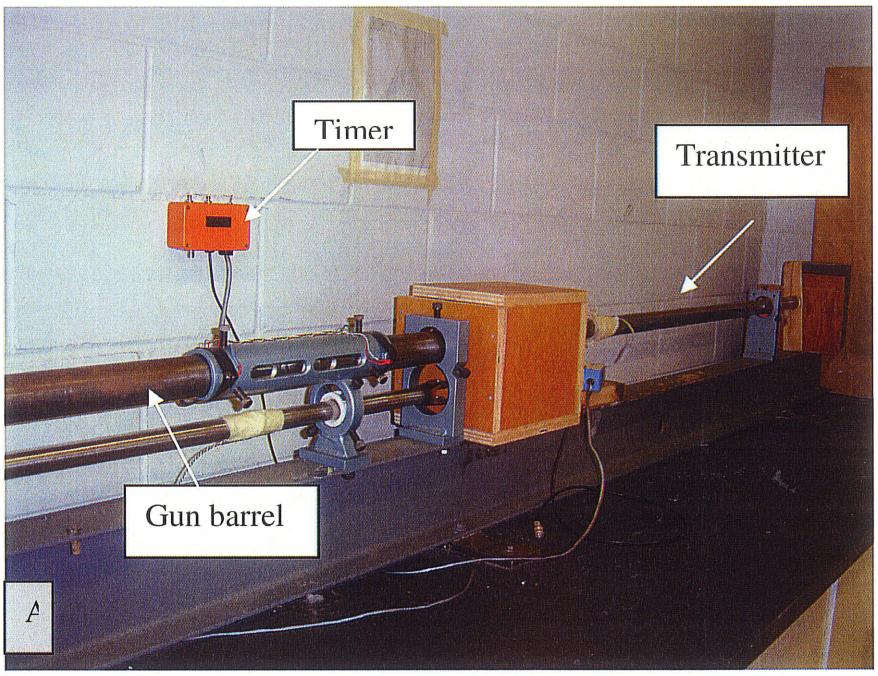

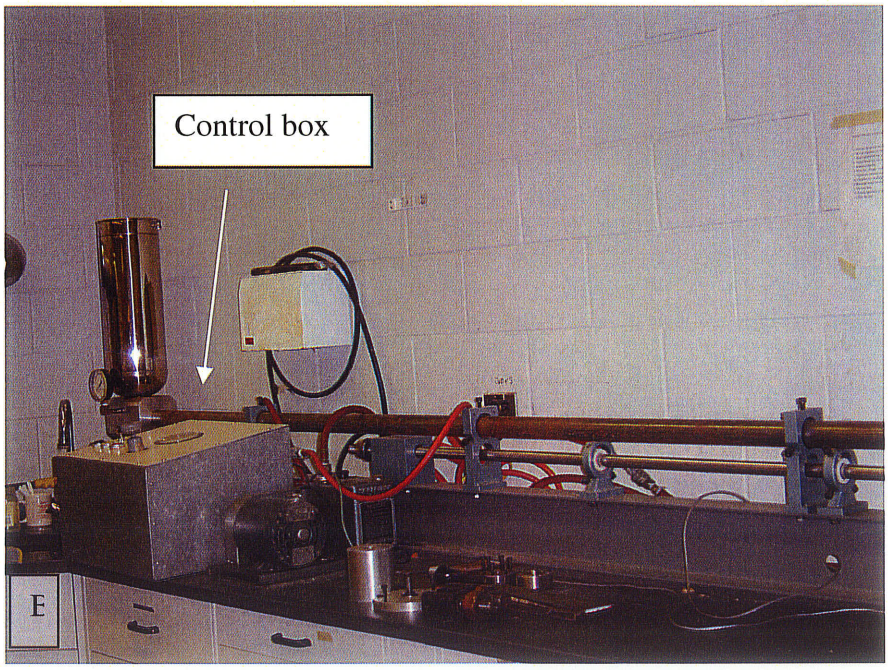

Fig 3.4 (A) right view of the Hopkinson Bar, (B) left view of the Hopkinson Bar

3.4.2 Impact procedure

The test pieces in as-tempered condition were subjected to high strain-rate deformation using the Split Hopkinson Pressure Bar (SHPB). The schematic view of compressional SHPB used in this investigation is presented in Fig. 3.4. A light gun fires a cylindrical projectile that travels through the gun barrel and strikes the specimen at a very high impact velocity, generating elastic waves, which travel through the specimen and are transmitted onto the output bar (transmitter). The firing pressure was varied to obtain different velocities at which the projectile strikes the test piece. A strain gauge connected to the output bar at about 30 cm from the impact receiving end of the output bar captures the strain signal in form of elastic waves transmitting through the bar. A strain pulse amplifier amplifies the strain signal and sends it to an oscilloscope, which collects and stores the strain data. The oscilloscope captures the strain signal in form of voltage against time. Equipment calibration under quasi-static loading conditions shows the correlation between the measured voltage and the corresponding load as follows:

$$P = 1.6396\,V \tag{3.1}$$

Where P is load in KN and V the measured voltage in mV. Assuming constant volume and linear variation of displacement with time and constant strain rate, the true stress (σ) and true strain (ε) at time t_s are given by the following expressions [18]:

$$\sigma(t_s) = \frac{P(t_s)}{A_i} \frac{L_i - (L_i - L_f)(t_s/t_f)}{Li} \quad (3.2)$$

$$\varepsilon(t_s) = \ln \frac{L_i}{L_i - (L_i - L_f)(t_s/t_f)} \quad (3.3)$$

Where P (t_s) is Load at time t_s, L_i and L_f are original and final lengths of the specimen respectively, A_i is the original cross section area and t_f is the total time of deformation. The strain rate ($\dot{\varepsilon}$) is given by the slope of the strain- time curve:

$$\dot{\varepsilon} = \frac{\partial \varepsilon}{\partial t} \quad (3.4)$$

3.5 Metallography

Sample preparation for metallographic investigation of the impacted samples involves sectioning, mounting grinding, polishing and etching. The samples were cut both in transverse and longitudinal sections in order to have a clear picture of the geometry of the adiabatic shear bands in the impacted cylindrical steel specimens.

3.5.1 Samples Preparation

Mounting is an important step for preparing samples for metallographic investigations. Small size specimens are difficult to handle during grinding and polishing operations. Mount thickness is important because very thick samples are hard to keep flat during grinding and polishing processes, while thin samples are hard to handle. Cleaning of the specimens is necessary before mounting for edge retention.

Plastic mounting of metallographic samples can be divided into two types. First type needs pressure and high temperature to fuse powder material into a solid mass around the samples. The second type involves mixing two polymeric liquid at room temperature and allows settling around the samples in a mould. The first type of plastic mounting procedure was used in this study and the molding powder was black bakelite phenolic powder, the mounting temperature and pressure were 130°C and 4.2 MPa respectively. The elevated temperature and pressure inside the mould chamber allows compaction and melting of the black bakelite around the samples forming a cylindrical plastic mount as shown in Fig. 3.5. This process is followed by grinding and polishing of the samples in order to obtain the mirror like surface. Polished samples were etched using the 2% Nital to reveal the surface microstructure when viewed under the optical microscope.

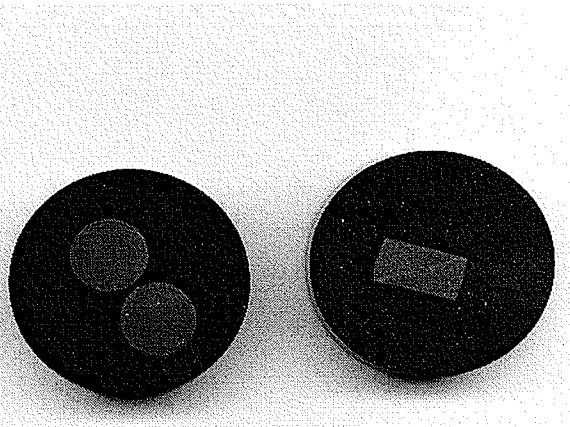

Fig 3.5: Plastic Mounting

3.6 Specimens Investigations

3.6.1 Microstructure Analysis

The prepared samples were investigated using both optical and scanning electron microscopes, Zeiss optical microscope with the Clemex Vision Analyzer and JEOL JSM-5900 LV Scanning Electron Microscope with applied voltage of 20 V were used in this study.

2.6.2 Microhardness Measurement

The micro-hardness test was based on the Vickers method (HV). The equipment used was Letz Wetzlar microharness tester . A 136° pyramids diamond indenter was used to form square indent inside and outside the shear bands. 50 gm load was used to form the indent depending on the metal hardness. The load was applied for 10-15 second to allow the indent to form. On removing the indenter, the lengths of the two diagonals using microscopic lens guided by small ruler were measured. Tables are available that give the Diagonal Pyramid Hardness (DPH) values corresponding to the measured indent diagonal. The DPH is related to the indent diagonal by the following expression:

$$DPH = \frac{\text{Constant x Applied Load}}{(\text{Indent Diagonal})^2} \qquad (3.5)$$

To compare the hardness inside and outside the shear bands regions, the indents were located in both regions as shown in Fig. 3.6

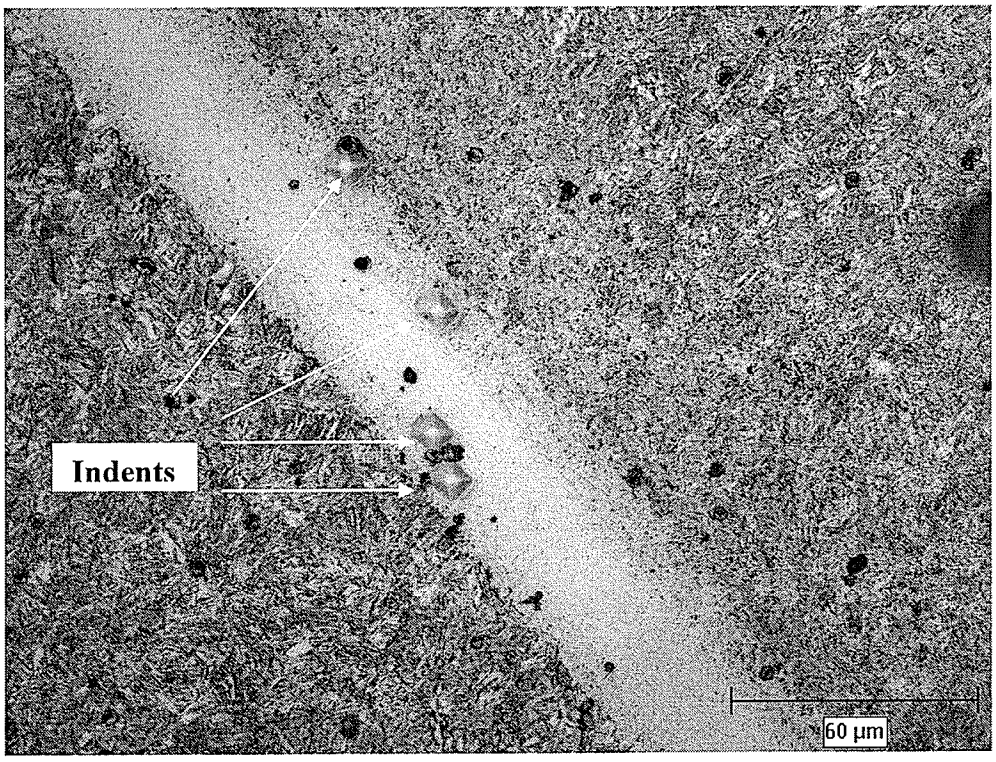

Fig.3.6: Photomicrograph showing indents formed in the shear bands during microhardness testing

3.7 Post Impact Heat Treatments

Some of the test samples were sectioned and heat treated for a time period ranging between 20 minutes and 2 hours at elevated temperatures of 315, 400, 500, 600 and 650 °C. The purpose of this annealing treatment is to reverse the microstructural transformation accompanying adiabatic shearing and eliminate the deleterious effect of adiabatic shear bands on the mechanical properties of the materials. It is intended to investigate how the heat treatment variables such as temperature and time influence the structure and properties of adiabatic shear bands. A survey of literature suggests that adiabatic shear bands consist of sub-grains of order of a few hundreds of nm and high density dislocations. The high temperature treatment is intended to reduce the dislocation density in the adiabatic shear bands, trigger coarsening of the extremely fine sub-grains in the shear bands, and ultimately leading to an improvement on the ductility and damage resistance as well as tolerance of adiabatic shear bands.

CHAPTER FOUR: RESULTS AND DISCUSSION

4.1 Results

4.1.1 Dynamic stress-strain curves

The stress-strain data were calculated from the raw data captured by the oscilloscope during impact test using equations (3.1- 3.4). Typical stress-time and stress-strain curves for the samples during impact loading are presented in figures 4.1 and 4.2 respectively. Both the strain (ε) and strain rate ($\dot{\varepsilon}$) increase with deformation time. The strain rate increases almost linearly as the strain increases from the inception to the end of deformation. The curves show clear yield point, which signals the onset of plastic deformation. Strain hardening effect of the plastic deformation dominates the deformation process until a maximum flow stress (σ_{max}) is reached. Beyond the maximum flow stress, the thermal softening begins to play the major role in the deformation process. Consequently, the flow stress decreases progressively with further increase in strain. As strain increases, a critical strain ($\varepsilon_{crit.}$) is reached where a sharp drop in stress is noticeable, indicating stress collapse due to rapid thermal softening effect of adiabatic heating leading to strain localization.

The strain rate depends on the velocity at which the projectile strikes the test specimen. The firing pressure was adjusted to produce different projectile velocities. The higher the impact velocity, the greater is the amount of deformation at any given time (ε_t) and the greater is also the rate of deformation

(Figs. 4.3 and 4.4). The effects of impact velocity on the flow stress for samples that were tempered at 315 °C as a function of time, strain and strain rates are presented in Figs. 4.5 and 4.6. The average strain rate of the samples that were deformed by projectile striking at impact velocities of 20.5, 22.49, 30.15 and 30.29 m/s were calculated to be 998, 1092, 1380 and 1420 s^{-1} respectively. Depending on the impact velocity, the average strain rates varied between 800 and 1100 s^{-1} at the inception of deformation and between 1240 and 1850 s^{-1} just before the completion of the deformation process. The higher the impact velocity (strain rate), the greater is the yield or maximum attainable flow stress.

The effect of strain rates on the adiabatic shearing in specimens tempered at 315 °C shows that the higher the strain rate, the shorter is the time for the commencement of stress collapse and strain localization. Depending on the impact velocity, the critical strain for adiabatic shearing lies between 0.38 and 0.45. The stress-strain and stress-time curves for samples tempered at 425 °C are presented in Figs. 4.7 and 4.8. For about the same impact momentum of the projectile, the total strains for these samples are generally lower than those for the samples that were tempered at 315 ° C. The average critical strain and time for strain localization was found to be about 0.16 and 242 μs respectively, which are also lower than for samples tempered at 315° C. These results suggest that the time and critical strain for commencement of strain localization do not only depend on the strain rates, they are also influenced by the microstructure of the steel.

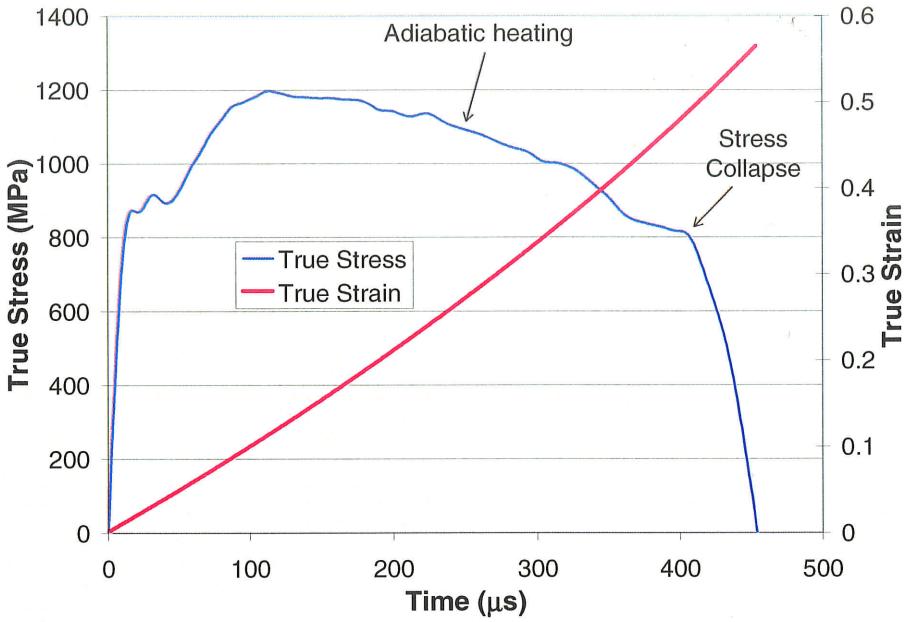

Fig. 4.1: Typical dynamic stress-time and strain-time curves obtained from the impact tests

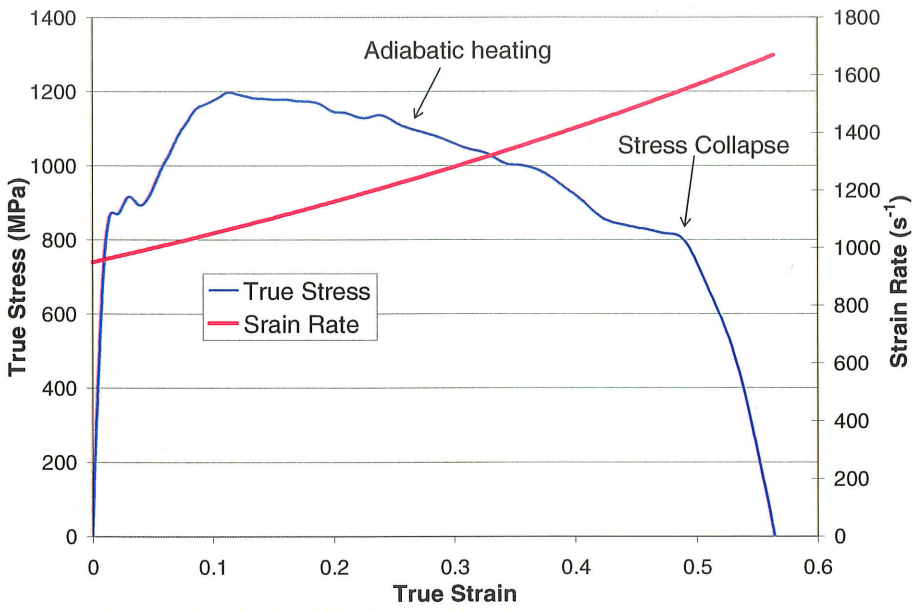

Fig. 4.2: Typical stress-strain curves and strain-strain rate curves obtained from impact test.

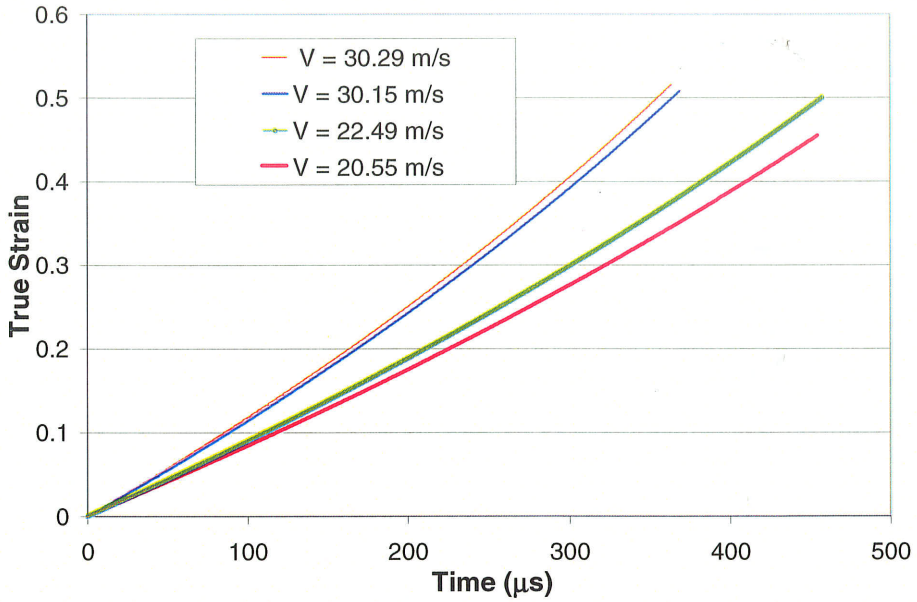

Fig. 4.3: True strain as a function of deformation time and impact velocity

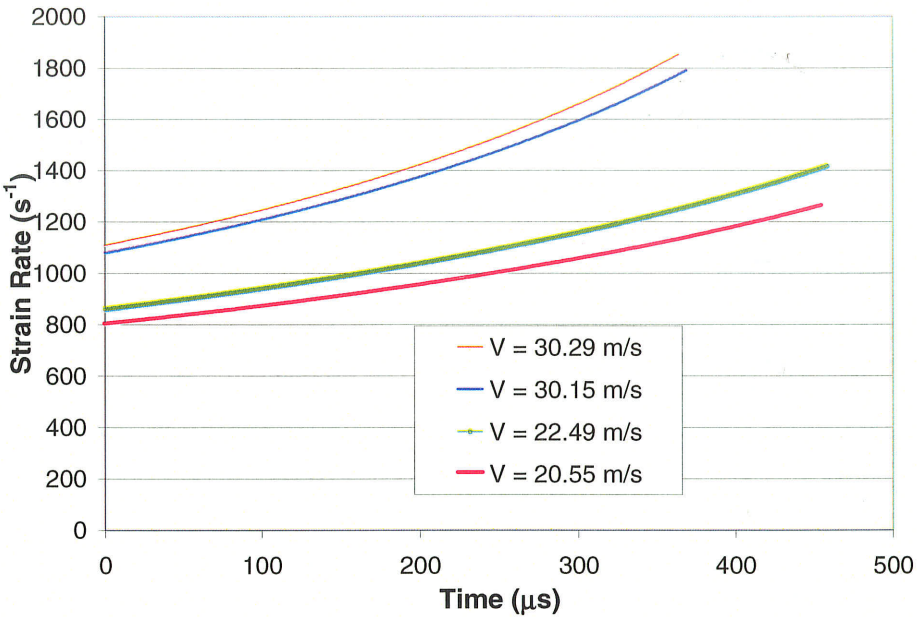

Fig. 4.4: Strain rate as a function of impact velocity and time

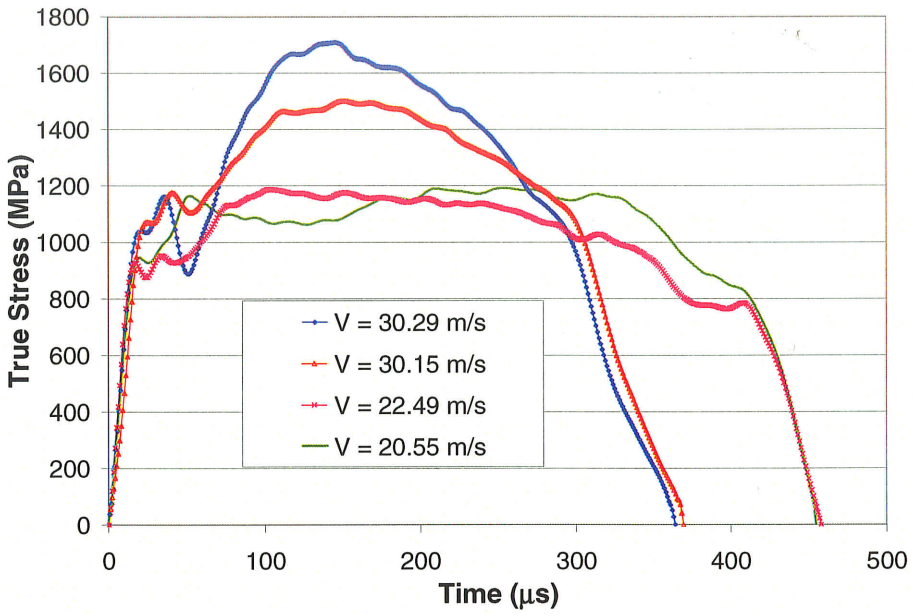

Fig. 4.5: The dependence of true stress- time curves on impact velocity

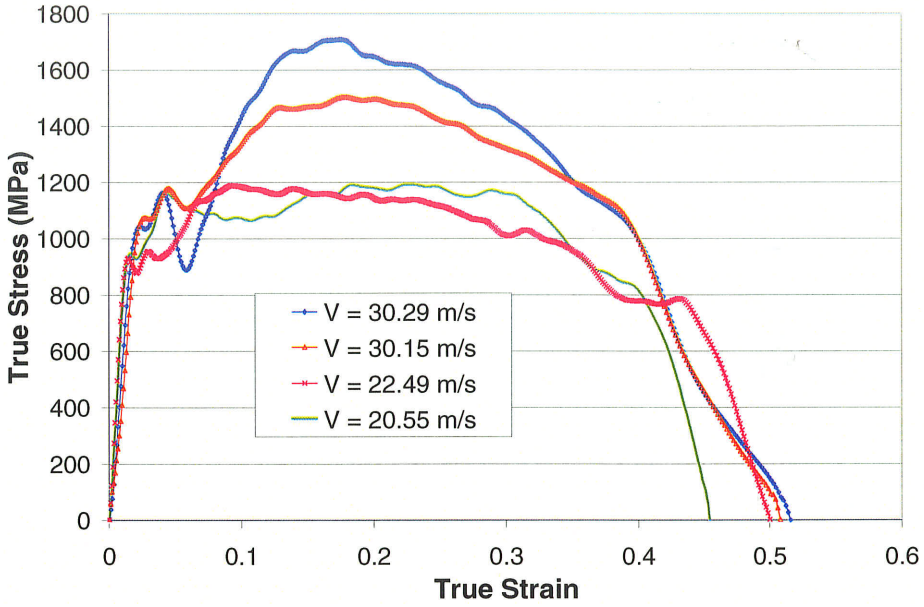

Fig. 4.6: True stress-strain curve as a function of impact velocity

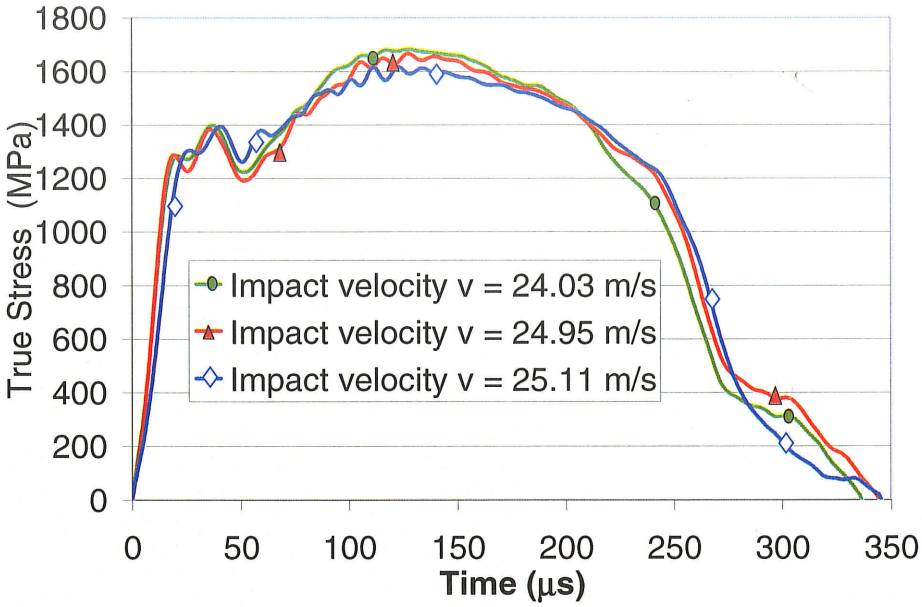

Fig. 4.7: True stress-time curves for samples tempered at 425 °C

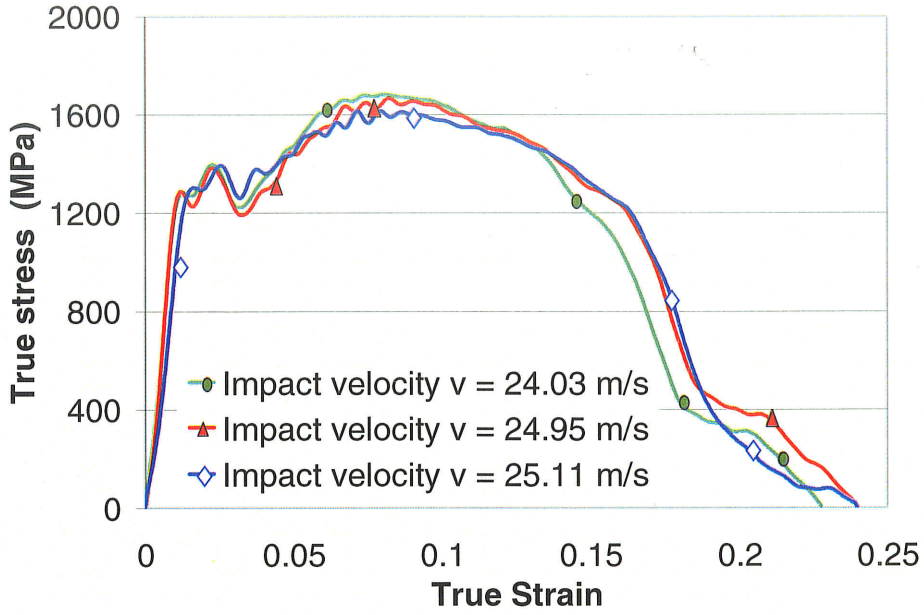

Fig. 4.8: True stress-true strain curves for samples tempered at 425 °C

4.1.2 Microstructural evaluation of the samples after deformation

Optical microscopic examination of the samples after impact test shows formation of distinct adiabatic shear bands which appears mainly as white bands on polished surfaces of impacted specimens after etching with nital (Fig. 4.9). The width of the white etching bands varies along the path of propagation between 50 and 80 μm. The width of shear bands during formed adiabatic shearing is assumed to adjust itself so as to achieve maximum growth rate. The direction of flow pattern around the white etching band can be noticed around the white etching band. The viscous flow pattern band becomes less noticeable with distance away from the shear band, suggesting the thermal softening around the white etching band reduces gradually with distance from the shear band. Layers of deformed band on both sides of the white etching bands form the transition region between the white shear bands and the bulk material.

As a result of the adiabatic shearing during impact the circular cross section of the samples assumed elliptical shape after impact. When observed under the stereo microscope at low magnification, the adiabatic shear band forms a circular propagating path as in Figure 4.10. Except in the regions where there are significant distortions in the geometry of the sample, the circumference of the shear band is very close to the edge of the cylindrical samples on transverse sections near the impacted surface. The diameter of the shear bands decreases with distance from the impacted surface.

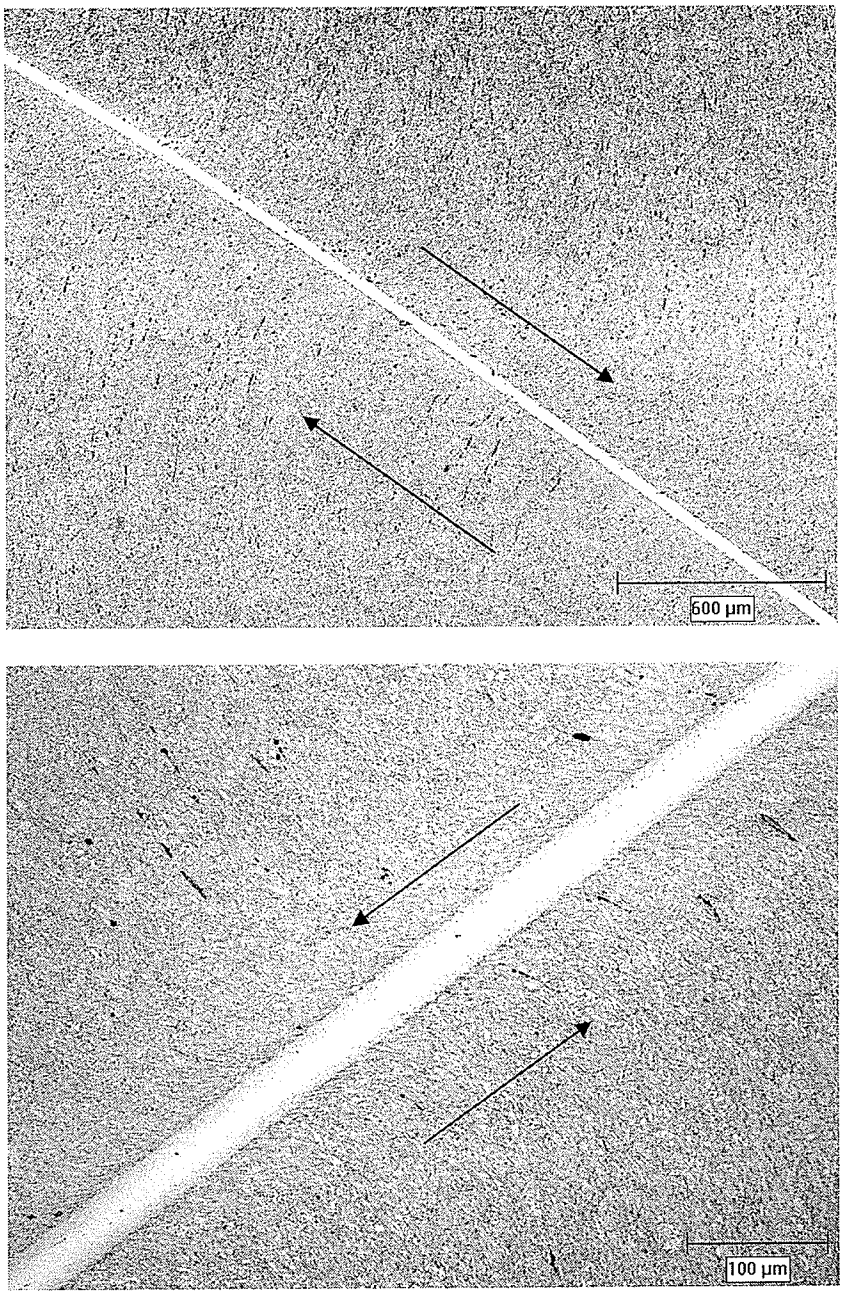

Fig. 4.9: Optical micrographs shown white etching ASBs formed during high strain deformation of the investigated steel samples. Arrows show the shear flow pattern in the regions adjacent to the shear bands

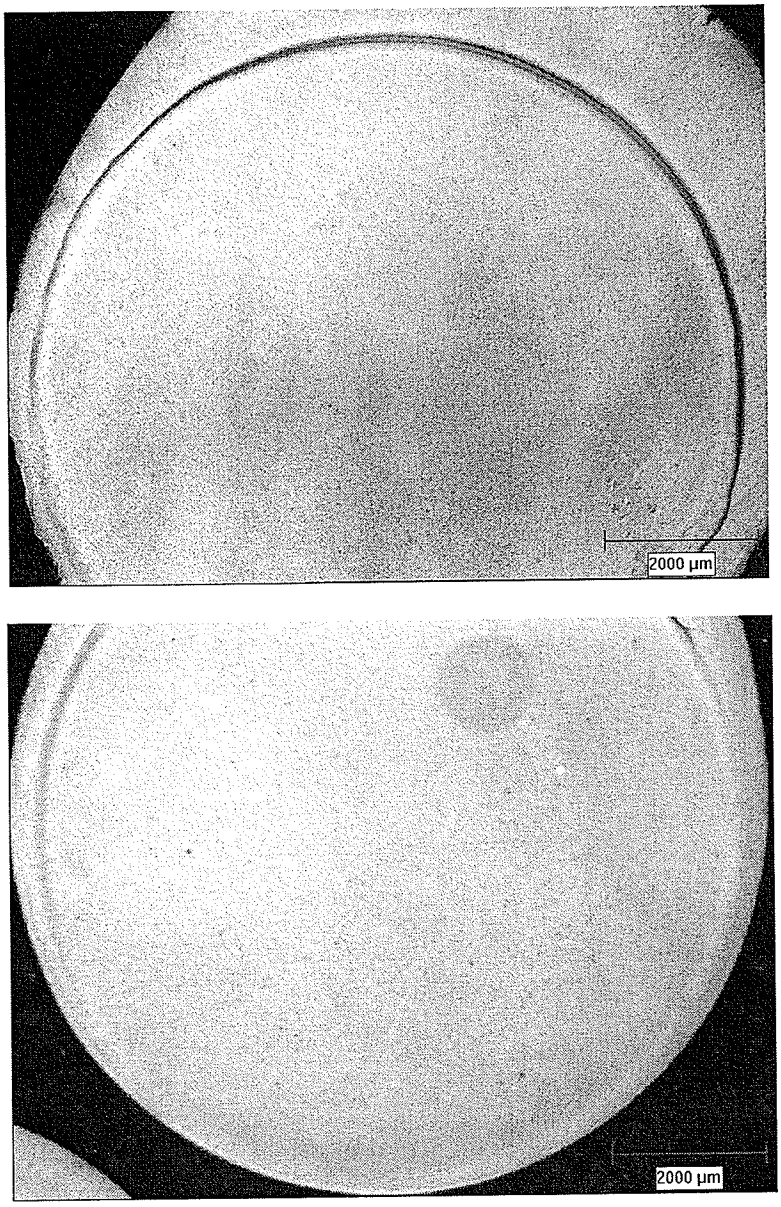

Fig. 4.10: Macrostructure of transverse section of impacted sample showing the circular geometry of the adiabatic shear band

Figure 4.11a shows typical macrostructure of the longitudinal section (cut parallel to the direction of the applied impact loading) of the impacted samples as seen under the stereo microscope. Two bands displaying parabolic shape with one appearing as the inverse of the other can be observed on the section. The curve path traced by the shear band in longitudinal sections at higher magnification when observed under optical microscope is presented in Fig 4.11b. It is evident from the geometry of the adiabatic shear bands in the transverse and longitudinal sections that adiabatic shear bands propagate in three directions during the rapid deformation forming two identical cones inside the cylindrical specimen. A schematic representation of the geometry of the shear band inside the test specimen is given in Fig. 4.12. The cones that extend outwards from the centre of the specimen towards the bottom or top of the cylindrical specimens are symmetrical and appear as mirror image of one another.

When observed either in transverse or longitudinal section, the adiabatic shear band propagation paths are usually very smooth curves for samples tempered at 315 °C before impact as shown in Fig. 4.13. However, most of the shear band's propagation paths that were observed in steel samples tempered at 425°C were characterized with bends and contours as shown in Fig. 4.14.

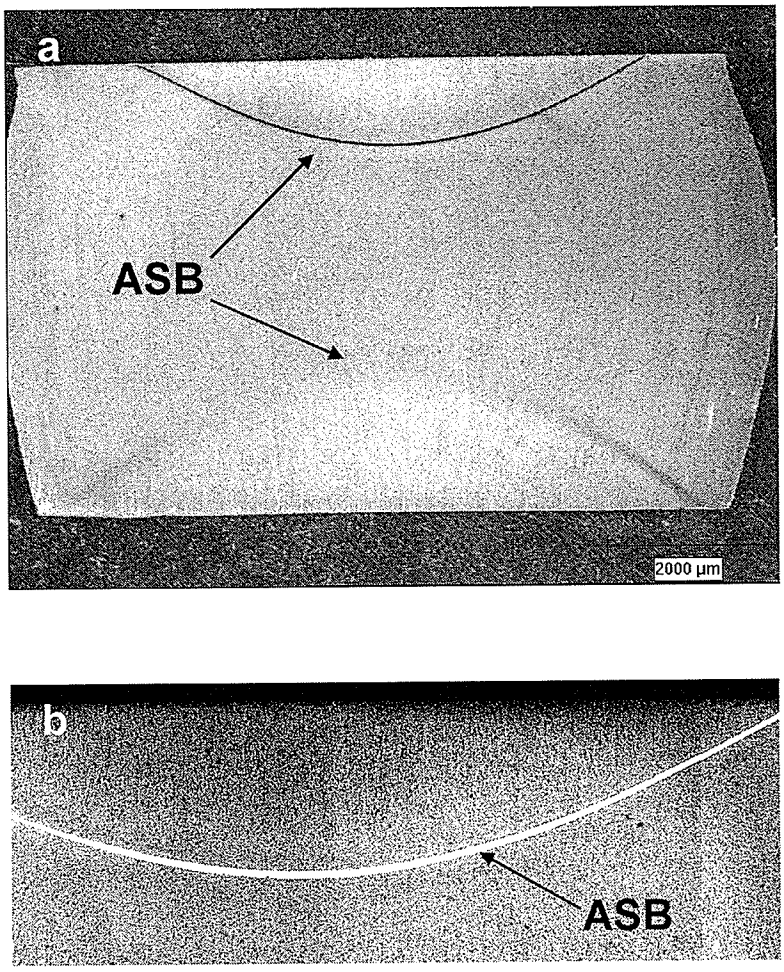

Fig 4.11: Geometry of adiabatic shear bands in the longitudinal section of the cylindrical test specimen. (a) Macrostructure as seen under stereomicroscope (b) microstructure as captured by optical microscope at magnification of (50X)

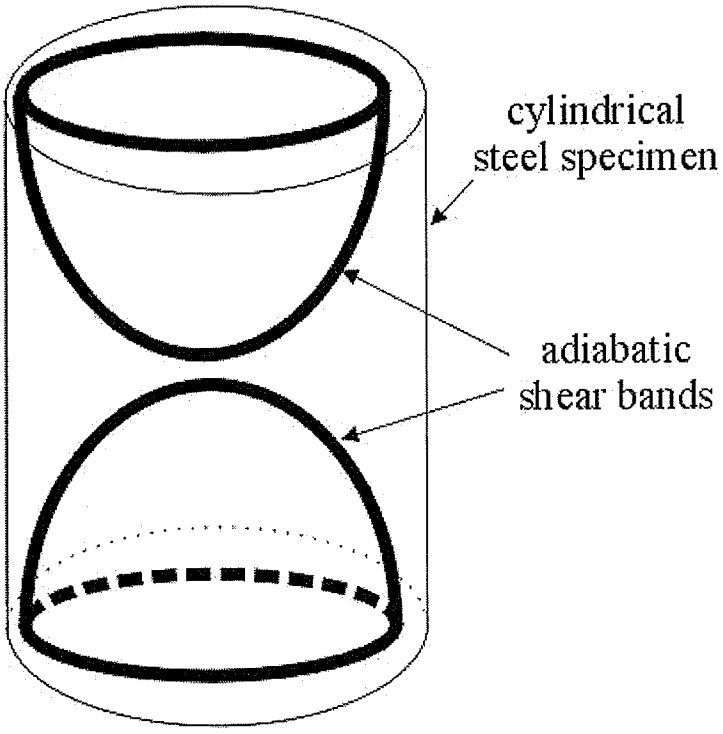

Fig. 4.12 Schematic representation of adiabatic shear bands propagation in cylindrical specimens.

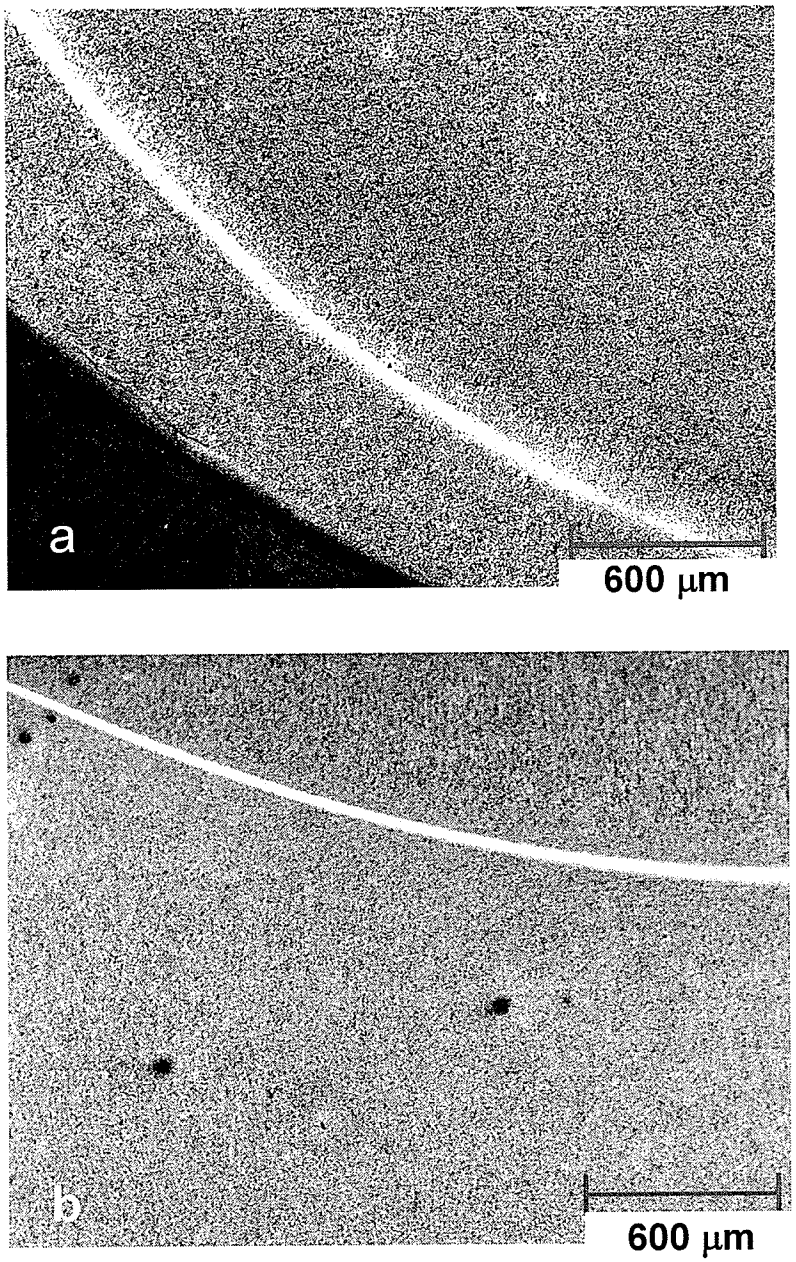

Fig. 4.13: Optical micrograph showing smooth propagation path of adiabatic shear band in samples tempered at 315 °C (a) transverse section (b) longitudinal section

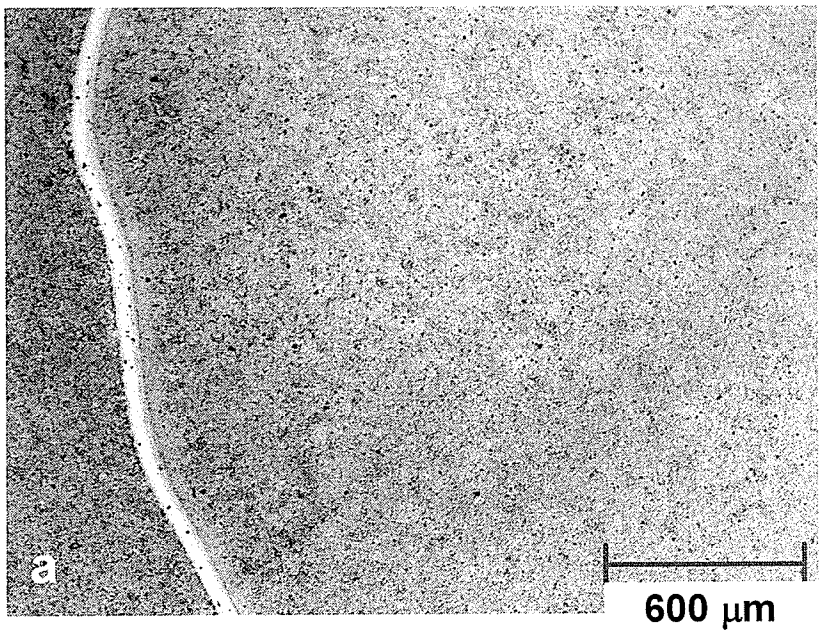

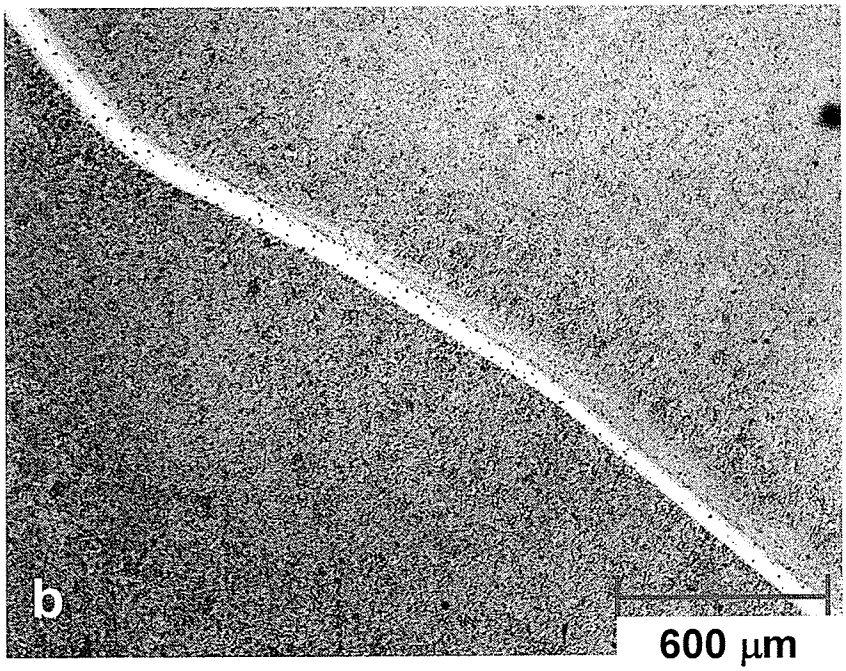

Fig 4.14: Optical micrograph showing contour and bends in the shear bands propagation path in steel tempered at 425 °C
(a) Transverse section (b) Longitudinal section

Single shear bands were observed to propagate along a circular path in the transverse sections of samples tempered at 315 °C while double or triple shear bands were observed in the transverse sections of many of the steel sample tempered at 425 °C as shown in Fig. 4.15. Where multiple shear bands were formed, the circles formed by the shear bands were concentric circles with their centre coinciding with the centre of the impacted cylindrical specimen. Of the multiple shear bands formed in the transverse sections of samples tempered at 425 °C, the one farthest from the edge of the cylindrical test specimens are white etching bands while the other bands close to the edge of the specimens are more like deformed bands than white etching bands. They have the same color and appearance as the bulk material but the plate-like structure of the bulk material could not be resolved in the deformed band.

As mentioned earlier the adiabatic shear bands, when observed in the transverse section of the impacted samples, have a circular shape. In most of the samples, a small fractional part of the circular shear bands is deformed bands which do not display characteristic white color of white etching band as shown in Fig. 4.16. Adiabatic shear bands serve as precursor and preferential crack initiation sites during dynamic loading. In some samples, rapidly propagating shear bands were observed to transform into cracks which cause fracture of some of the samples under impact. Figure 4.17 shows fully developed cracks propagating along adiabatic shear bands in some of the investigated samples as observed under the optical microscope after impact.

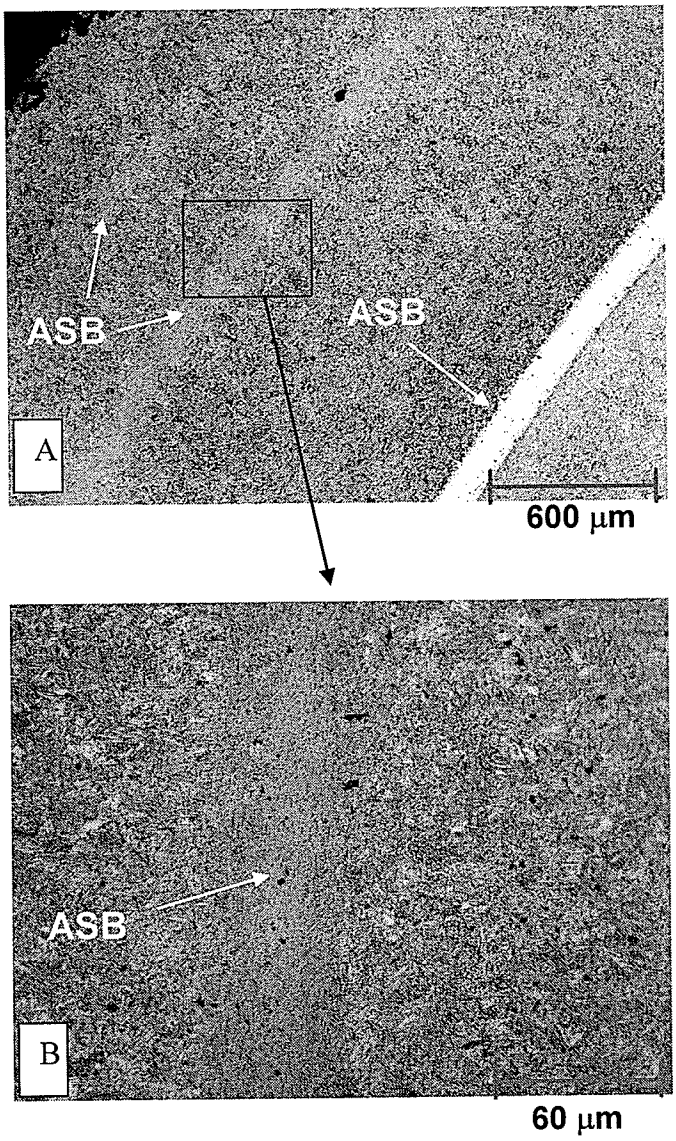

Fig. 4.15: Multiple shear bands in a steel sample tempered at 425° C.
Left hand corner of (A) is the edge of the sample.
(B) shows the secondary deformed band observed on
the transverse section at higher magnification (500 X).

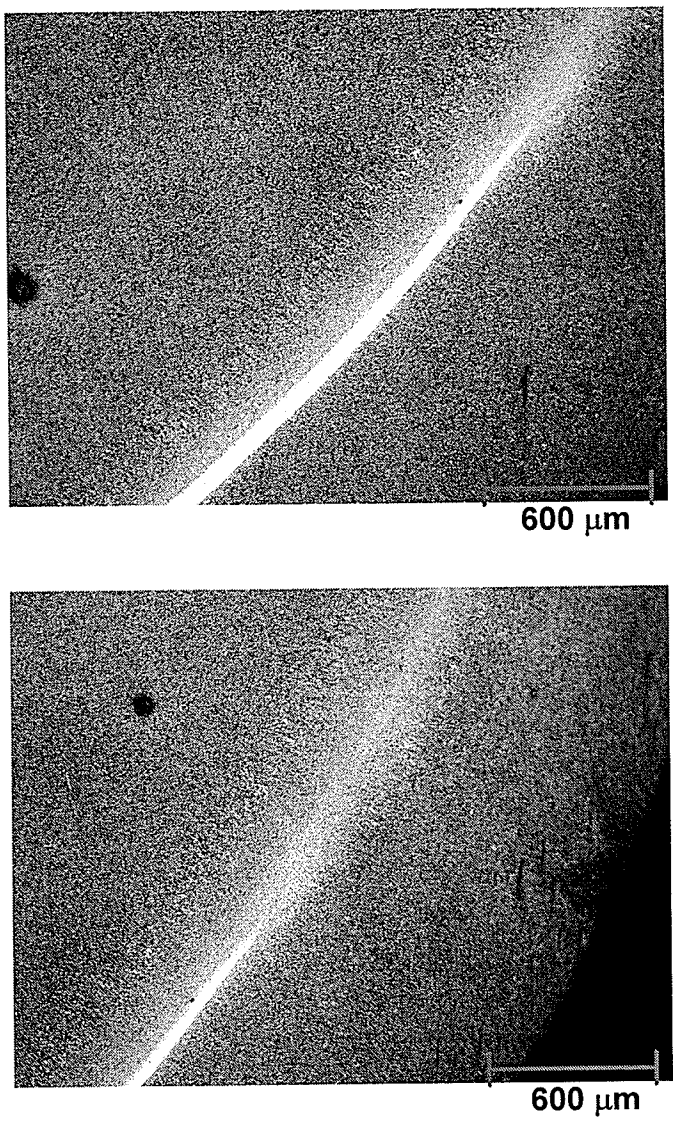

Fig. 4.16: Transformation of white etching band in to deformed band along the shear band propagation path in transverse section steel sample tempered at 315 °C

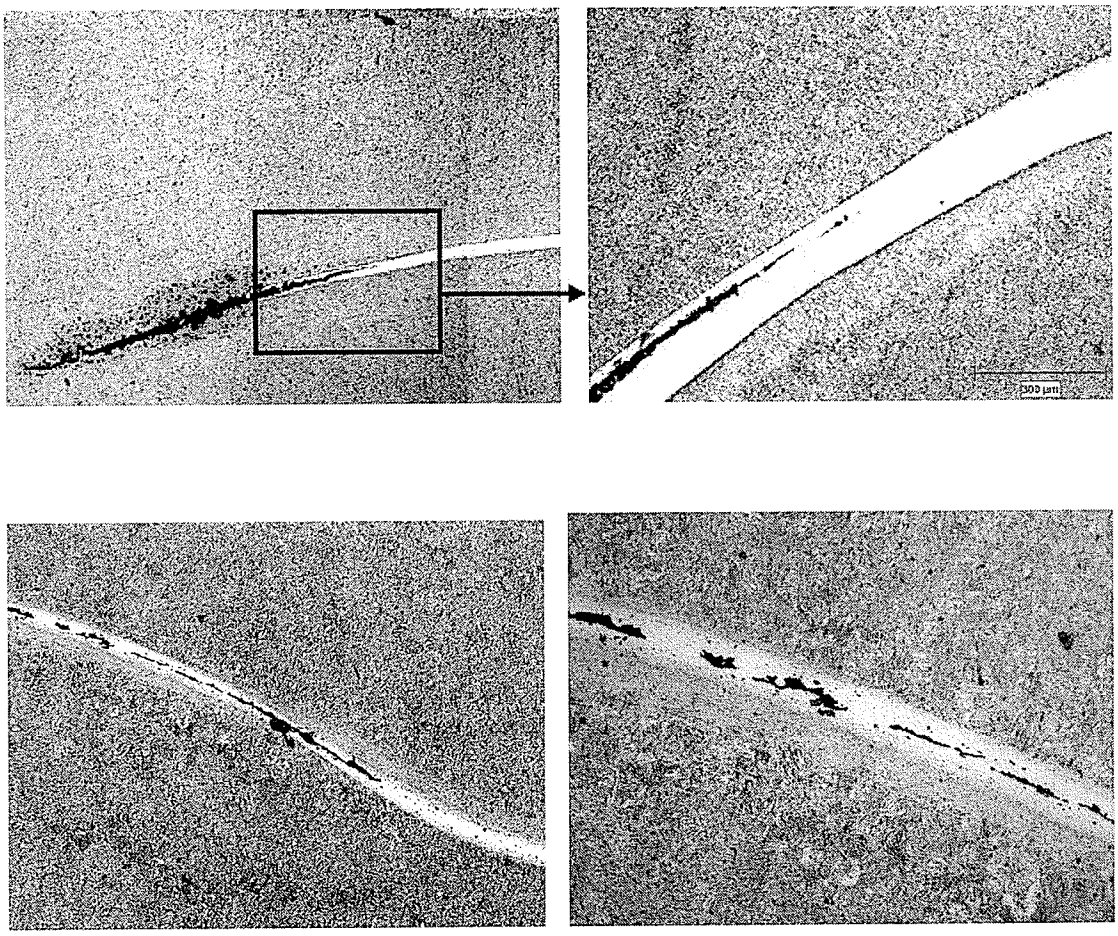

Fig. 4.17: Optical Micrographs showing cracking in adiabatic shear bands

The cracks in the shear bands were observed to initiate as a result of coalescence of voids which form in the shear bands during adiabatic shearing. Microcracks initiate and propagate along the direction of the shear bands at opposite sides of voids' clusters as shown in Fig. 4.18. Adjacent microcracks link together as deformation continues and develop into a full blown crack which propagate along the shear bands. Fig. 4.19 shows an undulating crack propagation path giving credence to the coalescence of voids as the mechanism for crack initiation and propagation. Some of the cracks in the shear bands penetrated into the bulk materials at some point where shear band rapidly change direction leading fragmentation of some of the samples into two identical pieces as shown in Fig. 4.20. Examination of the fractured surface shows that the samples failed by shear along adiabatic shear bands and the two cones formed by the shear bands in the test specimens are clearly noticeable on the fracture surface. A schematic representation of crack propagation path leading to fragmentation of samples into two identical parts is shown in Fig. 4.21.

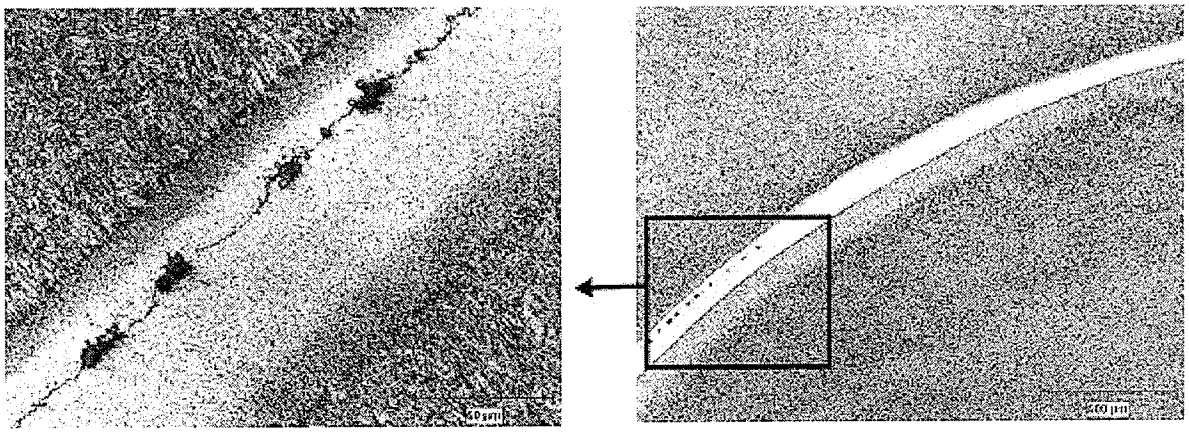

Fig. 4.18: Void formation preceding crack nucleation and propagation in the adiabatic shear band.

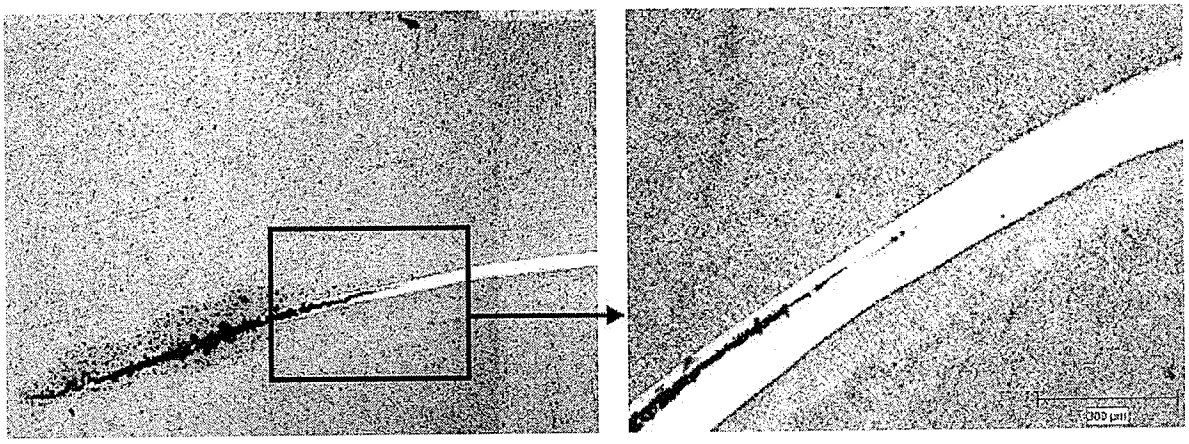

Fig. 4.19: A rapidly propagating crack during adiabatic shearing showing an undulating crack propagation path.

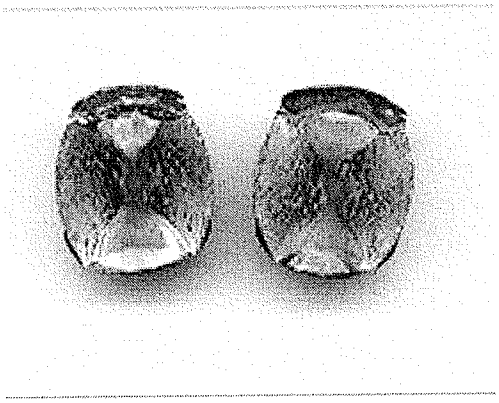

Fig 4.20: Photograph of a sample which broke into two identical fragments during impact showing the two cones formed by adiabatic shear bands before fracture

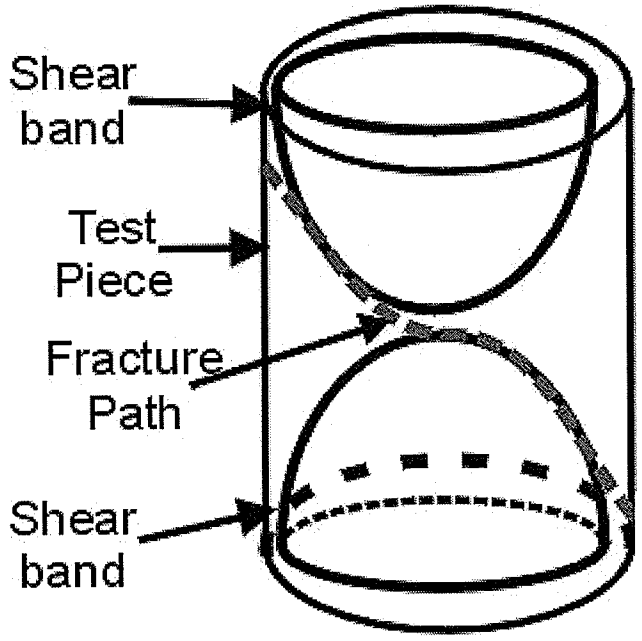

Fig. 4.21 Schematic representation of fracture path in failed samples during impact.

4.1.3 Micro-hardness test on samples before and after impact

The average hardness value of the sample before impact and of the bulk material outside shear band after impact was 350 DPH while the shear bands have average hardness value of about 620 DPH. The result of micro-hardness test shows that the shear bands are much harder than the bulk material (Fig. 4.22), a trend which can be traced to the very fine carbides and high dislocation density in the shear bands. The increase in hardness, as a result of high strain deformation of the samples, is concentrated in the shear band regions. No noticeable change was observed on the bulk material outside the shear bands. The high hardness of the shear bands make them more susceptible to cracking during subsequent mechanical loading, if cracking does not occur during adiabatic shearing. Formation of an adiabatic shear band can therefore be regarded as initiation of a damage mechanism in a material even if cracking does not occur during adiabatic shearing.

4.1.4 Effect of heat treatment on adiabatic shear bands

Effects of post impact thermal treatment

Heat treatment of the impacted samples at 315 °C for 2 hrs did not produce any significant change in the morphology of the shear band and that of the bulk material as observed under the optical microscope (Fig. 4.23). The adiabatic shear bands remain clearly distinguishable white etching bands as observed

before the thermal treatment. Figure 4.24 shows how the hardness of the shear band and that of the matrix vary with post impact thermal treatment. The hardness of the shear band was not reduced by heat treating at 315 °C for 2 hours. Instead, the hardness of both the matrix and shear band was observed to remain about the same within the limit of experimental error.

On soaking the impacted samples at 650 °C for 20 minutes, the white color of the shear bands disappeared as shown in Fig. 4.25. Although the shear band after this thermal treatment is optically distinguishable from the bulk material, it is very similar in appearance to the bulk material when viewed under the optical microscope. The shear flow pattern observed around the adiabatic shear bands after impact remains noticeable after the 20 minutes heat treatment at 650° C. SEM investigations of the samples after heat treatment at 650 °C shows spheroidized cementite embedded in a ferrite matrix as shown in Fig. 4.26. The hardness of shear bands decrease significantly to values slightly higher than the hardness of the impacted bulk material before heat treatment as shown in Fig. 4.24.

Prolonged heating of the impacted samples for 2 hrs leads to complete replacement of the white etching band with a deformed band that is hardly distinguishable from the bulk material when viewed under an optical microscope. The only distinguishing feature of the shear band region from the bulk material is the traces of flow pattern that indicates a prior massive deformation in that region

during impact. Figure 4.27 shows the optical micrograph of the sample after post impact annealing at 650 °C for 2 hrs. The hardness of both the shear bands and bulk material becomes even and approximately equal to that of the steel sample before impact as presented in Fig. 4.24. The microstructural changes that occur in the shear bands during adiabatic shearing have been reversed by high temperature treatment at 650 °C. The rather brittle white etching bands are replaced by a more ductile material that has the same level of hardness as the bulk material before impact.

The results of the investigation of the effects of one hour annealing on adiabatic shear band at 400, 500 and 600 °C are shown in Fig. 4.28. The results show that no significant change in the appearance of the adiabatic shear bands as observed under the optical microscope after one hour annealing at 400 °C. The adiabatic shear band retains its white color. However after one hour annealing at 500 °C, the white color of the adiabatic shear band has started to fade and is gradually being replaced by the grey color of the bulk material. After one hour heat treatment at 600 °C, the color of the adiabatic shear bands has changed completely from white to the grey color of the bulk material. The shear band under microscope appears like smooth surface. The grain boundaries or the plate-like structure of the bulk material could not be resolved with optical microscope. Unlike in the case of 20 minutes annealing at 650 °C, which completely transforms the white etching band into deformation band in which

deformation pattern and shear flow are visible, no such flow pattern is visible in the shear bands after annealing at 600 °C for one hour.

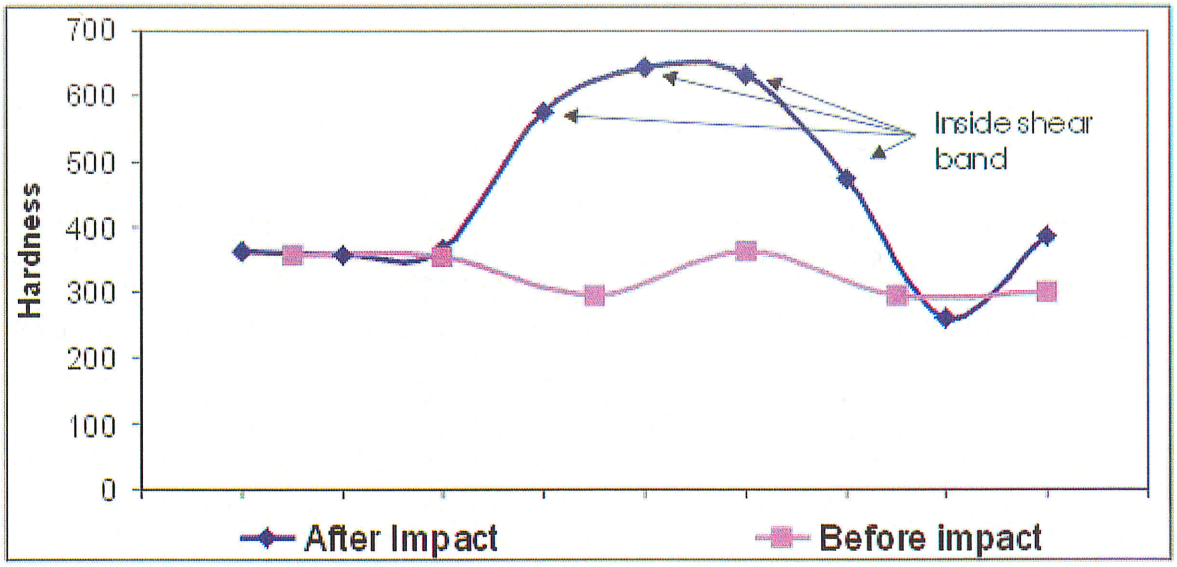

Fig. 4.22: Typical hardness distribution in the steel samples before and after impact.

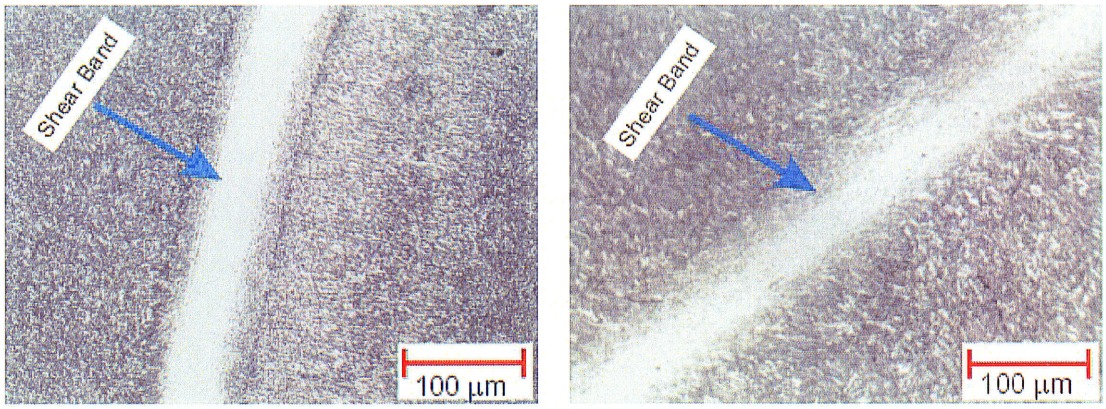

Figure 4.23: Optical Micrograph showing ASBs in impacted samples
(a) initial ASB, no post-impact heat treatment.
(b) impacted sample after annealing at 315 °C for 2 hrs.

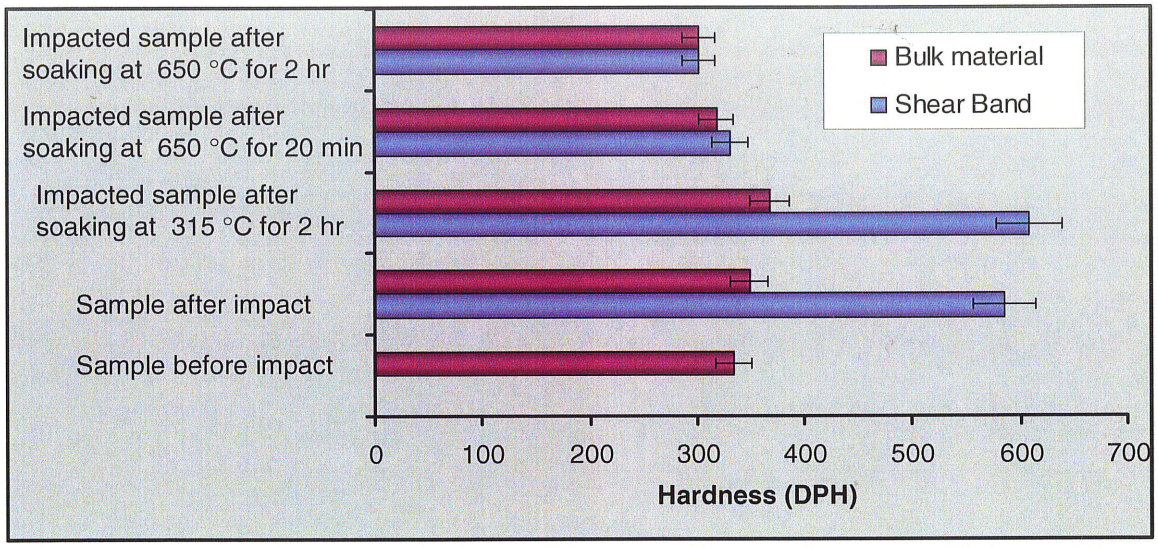

Fig. 4.24: Effect of post thermal treatment on hardness of ASBs and bulk material.

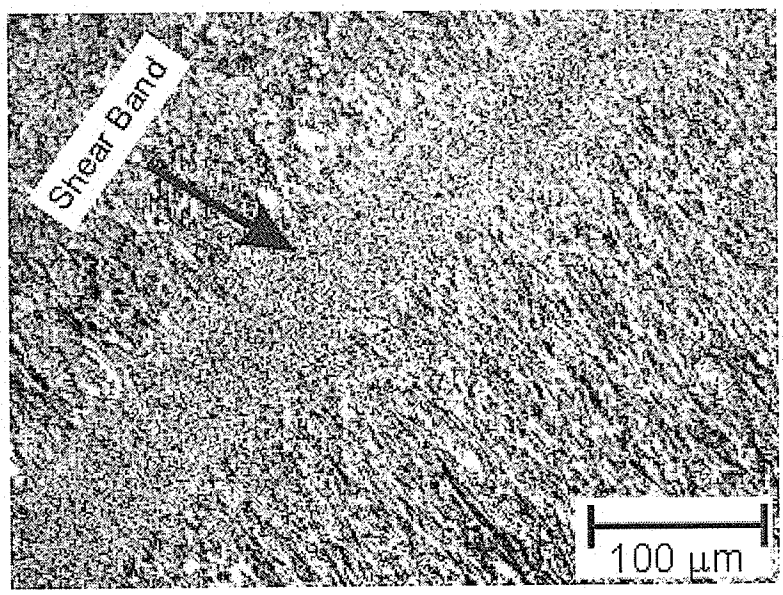

Fig. 4.25: Photomicrograph showing adiabatic shear band after post impact annealing at 650 °C for 20 minutes

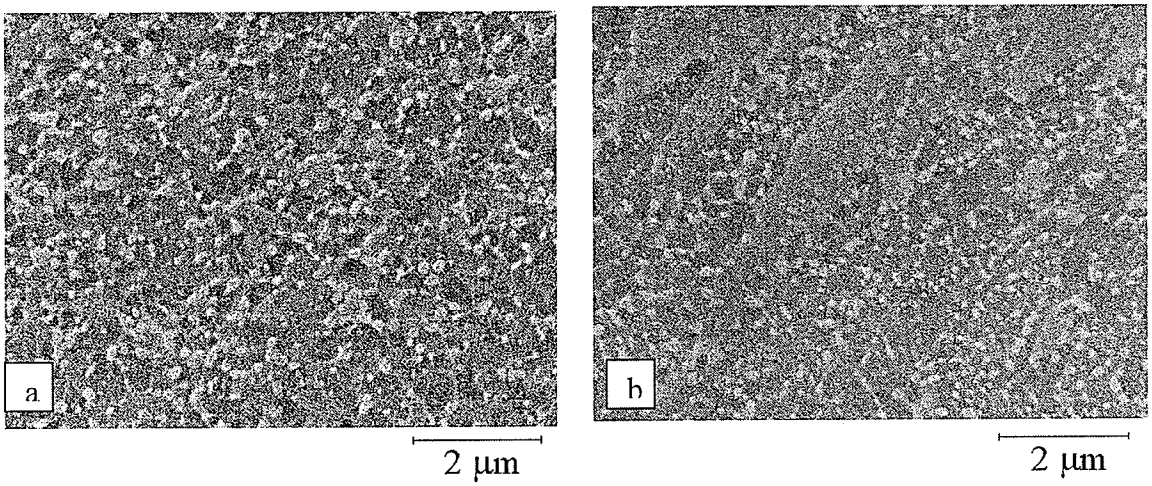

Fig. 4.26: SEM micrograph showing precipitation of carbides in the

(a) shear bands and (b) bulk material during annealing at 650 °C

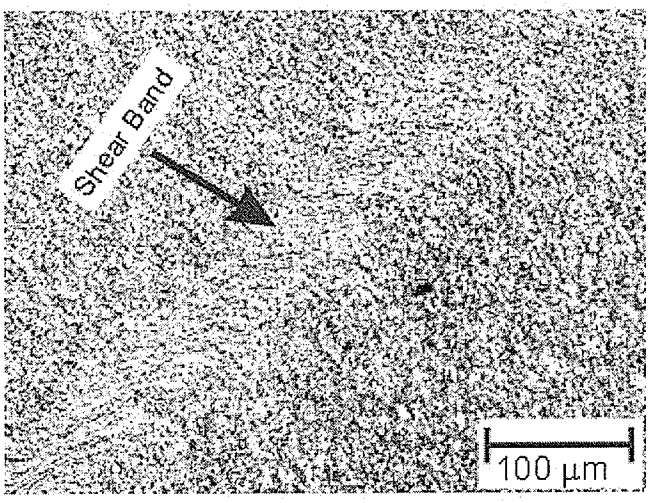

Fig. 4.27: The optical micrograph of the sample after post impact annealing at 650°C for 2 hrs.

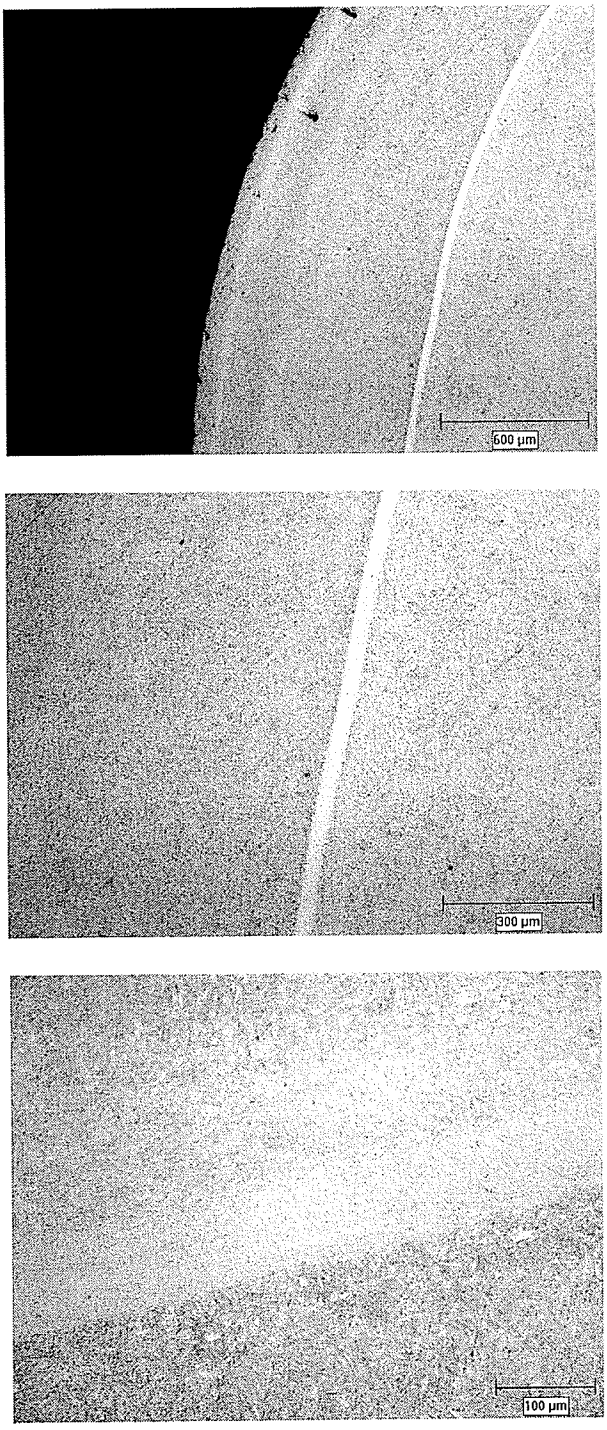

Fig. 4.28: Optical Micrograph showing the microstructure of the adiabatic shear band and bulk material after post impact thermal treatment for one hour at 400 °C.

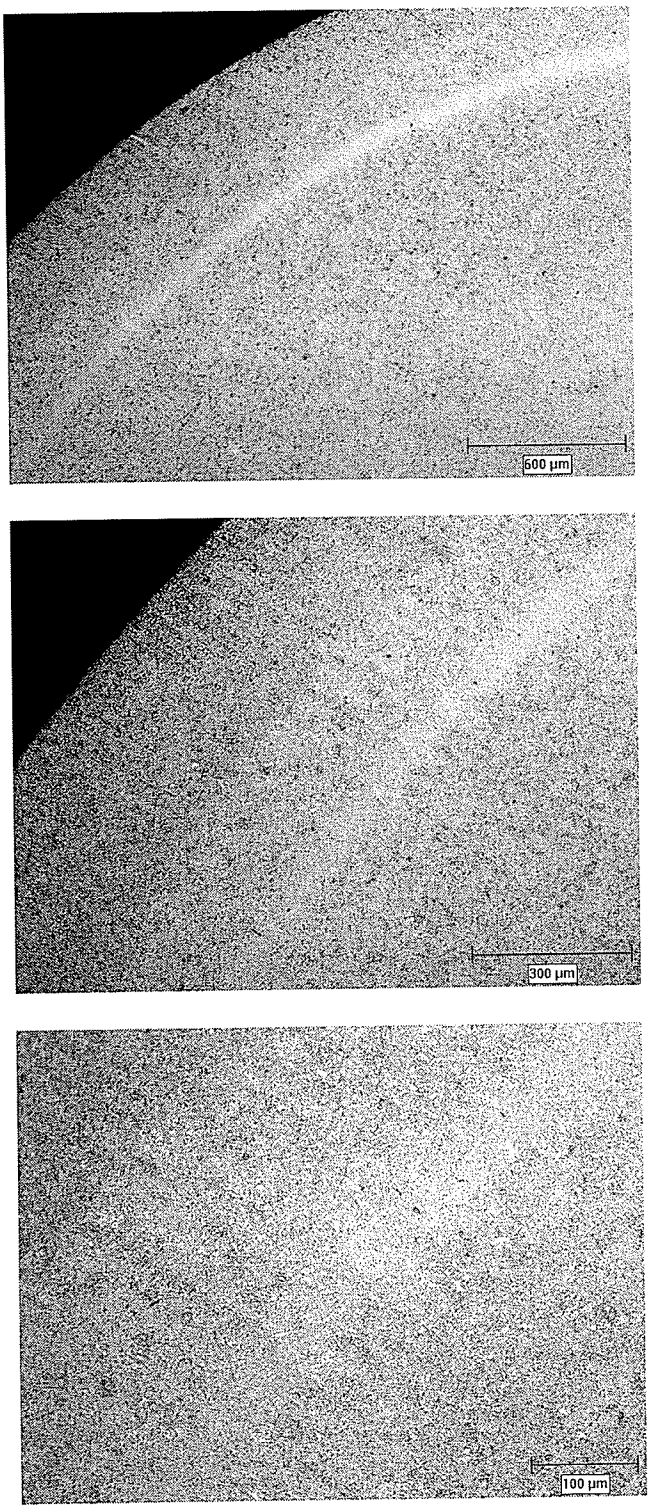

Fig. 4.29: Optical Micrograph showing the microstructure of the adiabatic shear band and bulk material after post impact thermal treatment for one hour at 500 °C.

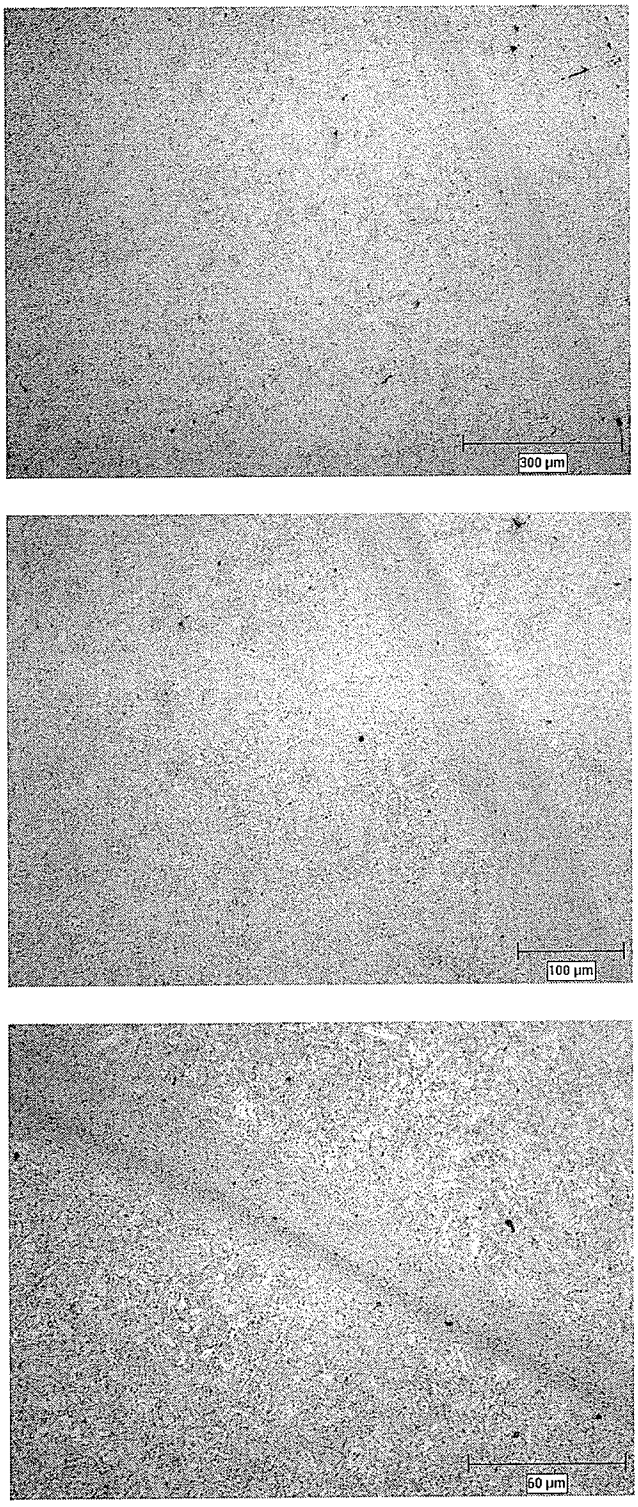

Fig. 4.30: Optical Micrograph showing the microstructure of the adiabatic shear band and bulk material after post impact thermal treatment for one hour at 600 °C.

4.2 Discussion

Results of this investigation show that stress collapse time and the critical strain required for stress collapse leading to mechanical instability, loss of load carrying capacity and ultimately to strain localization are significantly influenced by strain rates and microstructure. Schonefeld and Wright [14] gave inhomogeneous distribution of temperature as one of the perturbations that influence stress collapse time. The observed decrease in critical strain for shear localization, in the present study, as strain rate increases agrees with Ramesh's [5] observation that shear localization in tungsten heavy alloys is highly dependent on strain rate. The higher strain rate probably increased the perturbation, in the test specimen, which subsequently enhanced the chance of a speedy onset of stress collapse as soon as the adiabatic heating began. Culver [66] showed that the critical strain $(\varepsilon_{crit.})$ for the onset of strain localization is influenced by a number of variables as shown in the following model:

$$\varepsilon_{crit.} = \frac{n\rho C}{\beta \left| \partial\sigma / \partial T \right|_{\varepsilon,\dot{\varepsilon}}} \qquad (4.1)$$

where n is the strain hardening exponent, ρ is density of the material, C is the specific heat capacity, β is the fraction of deformation energy that is converted to heat, $\partial\sigma/\partial T$ is the slope of temperature dependence of flow stress taken at

constant strain and strain rate. This model implies that the $(\varepsilon_{cirt.})$ will be dependent on strain rate $(\dot{\varepsilon}.)$ for a material in which n , ρ , C are constant.

The lower stress collapse time and minimum strain needed for adiabatic shearing recorded for steels tempered at 425 °C in comparison to those tempered at 315 °C can be traced back to the microstructural transformation that takes place during tempering of alloy steel at the tempering temperature of 425 °C. Cho et al [21] suggested that the thermodynamic stability of microstructure may have an influence on the readiness of a material to experience stress collapse and strain localization. Consequently raising the tempering temperature ought to translate to shear localization at higher strains. However, at tempering temperature of 425 °C, tempere embrittlement resulting in segregation of impurities along grain boundaries can occur. The presence of these segregations in the microstructure will increase the microstructural defects and perturbations which promote initiation and propagation of adiabatic shear bands.

Increased perturbations or material defects in the samples tempered at 425 °C can thus account for the low stress collapse time and critical strain value for shear localization. Feng and Bassim [30] reported that the presence of material or geometrical defects enhance the formation of the adiabatic shear bands. Results of experimental studies by Duffy and Chi [22] also indicated that critical strain, at which stress collapse occurs, depends on the size of initial geometrical defects. The results of mathematically modeling of adiabatic shearing by Wright and Walter [28] suggested that the time of stress collapse depended on the size

of an initial perturbation. Therefore segregation of carbides along grain boundaries during tempering of alloy steels at 425 °C will promote microstructural defects that will enhance early initiation of adiabatic shear bands. This is in line with the suggestion by Marchand and Duffy [27] that shear bands are most likely initiated at a point in the test section and then propagate rapidly as deformation progresses.

As mentioned in Chapter two, there has been some controversy in the generally acceptable explanation for the white color of the adiabatic shear bands that form in steels during high strain deformation. It has been suggested that the white shear band is a product of austenite to untempered martensite during adiabatic shearing [20]. In this case, the heat generated during adiabatic heating is considered to be high enough to convert the structure of the steel to martensite which is subsequently quenched by the surrounding matrix. The suggestion of reverse martensitic transformation has also been made to be the actual transformation taking place during adiabatic shearing leading to formation of white ASBs in steels [15]. Considering the very short time involved in adiabatic shearing, it is most unlikely that both austenite formation and subsequent transformation to untempered martensite could have occurred. It is generally believed that carbides and martensites plates are broken down and dissolved during adiabatic shearing resulting in very fine carbides and martensites which are too fine to be resolved using optical microscopy.

Several TEM studies on white ASB in steel has shown that shear bands consist of very fine cells less than 100 nm in size [15, 23]. Witmann et al [23] reported that the white etching ASBs in an explosively deformed AISI 4340 steel consist of fine Fe_5C_2 carbides and very fine martensite laths and suggested that white etching forms because the dissolution of carbides changes the etching characteristics of the structure. The carbides were 5 to 150 nm in thickness and formed as films on the internal twin boundaries. In the transition region between the white ASBs and the matrix, cementite carbides with diameters varying between 5 and 200 nm were observed. The very fine microstructure observed in between the matrix and the white etching bands in the present study may therefore consist of these very fine cementites and fine highly deformed martensite lathes that are aligned in the shear flow directions. Investigations by Meyers et al [24] show that shear bands in stainless steels consist of two regions: one region comprises extremely fine grains 0.1- 0.2 μm, well defined grain boundaries as well as a low density of dislocations and another region having a glassy structure that was formed by a solid state amorphitization process.

The multiple ASBs observed in steel samples that were tempered at 425 °C can be explained by perturbation theory which has been used earlier to explain the low critical strain required for adiabatic shearing and the short stress collapse time. The presence of segregations, formed in the microstructure at the tempering temperature, offers many initiation sites for adiabatic shear bands and

enhances multiple adiabatic shear banding in these steel samples. The variation in the nature of the shear bands from the characteristic white shear bands to grey color similar to that of the matrix can be traced back to the intensity of the fragmentation and dissolution of carbide plates during adiabatic shearing. It is suggested that the adiabatic heating and strain rate in the band displaying white color is so intense as to completely dissolve the carbides into extremely fine cells that are optically not resolvable. On the other hand, the strain rate in the shear band displaying the characteristic grey color of the bulk material is sufficient to highly deform carbide plates and aligns them in shear direction. The deformed carbide plates have sufficiently reduced in size that they can easily be distinguished from the characteristic carbide laths in the bulk material.

The increased hardness in the shear bands can be attributed to the work hardening and grain refinement bands caused by massive localized plastic deformation in the band during impact. Grain boundaries usually act as barriers to motion of dislocations during plastic deformation. Increased grain boundary per unit volume as a result of grain refinement in the shear bands will therefore lead to higher resistance to plastic deformation and therefore to increased hardness. Increased numbers of dislocations in the shear bands can also result in dislocation interactions whereby the large amount of dislocations will hinder the motion of one another when shear stress is applied. Thus, the hardness and strength of the shear band should be expected to be higher than that of the bulk material. Meyers and Wittman [2] observed that increased hardness in shear

bands in low carbon steels does not depend on the impact velocity; Rogers and Shastry [48] observed that hardness in white etching bands in steel was dependent on carbon content.

In this investigation, it was observed that the hardness of the shear band remained unchanged after 2 hour annealing at 315 °C. This suggests that recrystallization process at this temperature is either non existence or extremely slow. It can also been inferred from experimental results that the recovery process taking place at 315 °C does not involve much dislocation climb and rearrangement that can lead to a decrease in hardness. The observed significant hardness reduction after 20 minutes annealing at 650 °C can be traced to nucleation and growth of spheroidal cementite in the shear bands as observed in Fig. 4.26. Spheroidization of cementite is promoted by the resulting decrease in surface energy. The marked reduction in hardness of the shear band can be traced to reduction in dislocation density as a result of recrystallization and growth of strain free and relatively coarse carbide grains during the heat treatment process. According to Hall-Petch equation the yield strength (σ_y) of a polycrystalline material decreases with increasing average diameter of the grains (d) as follows

$$\sigma_y = \sigma_o + \frac{K}{\sqrt{d}} \tag{4.2}$$

where σ_o and K are constants for the material.

A possible mechanism for the observed change in microstructures of the shear bands during the heat treatment operation at 650 °C is coalescence of dissolved extremely fine carbides inside the shear bands, [21,25,26,55], forming larger aggregates of spheroidized carbides that are observed in SEM investigations shown in Fig. 4.26.

An earlier transmission electron microcopy investigation on the recrystallization of cold rolled silicon irons has shown that strain free recrystallized nuclei are formed by coalescence of sub-grains at the most severely deformed portion of the grains. The atomic mechanisms for sub-grain coalescence forming new recrystallized grains involves re-orientation or rotation of sub-grains such that a sub-grain achieves the same orientation as one of its neighbors resulting in the disappearance of the boundary separating them. Consequently, larger size subgrains are formed without sub grain boundary migration [67-70]. Deformation induced grain coalescence occasioned by grain rotation was observed and reported in ultra fine grained aluminum (~20 nm) [71]. Paul et al [72] studied shear band recrystallization during annealing in brass, they observed that shear bands contain high angle boundaries and also noted that recrystallization of strain free grains occurs by coalescence of neighboring sub-grains.

Apart from subgrain coalescence, other possible mechanisms for coarsening of cementite particles in the shear bands may be subgrain growth, in which low angle grain boundaries of the subgrains are able to move through the material by

a process of climb and rearrangement, leading eventually to formation of a nucleus and the subsequent grain growth [69]. It has been reported that shear bands have high angle boundaries which are able to migrate and form nucleus [71]. The nucleation rate ($\dot{N}$) during recrystallization depends on temperature (T) and activation energy for nucleation (Qn) according to the Arrhenius equation:

$$\dot{N} = ke^{\frac{-Q_n}{RT}} \tag{4.3}$$

The recrystallization rate ($\dot{N}$) increases with increasing temperature and decreasing activation energy for nucleation. Activation energy decreases with increasing strain and decreasing initial grain size. This implies that the high strain and very fine nature of the particles in the shear bands can enhance the rate of recrystallization of new stress free carbide grains at the heat treatment temperature. Nucleation and growth of strain free relatively coarse carbides grains from the very fine nanosized carbide subgrains in shear bands resulted in the observed decrease in hardness as reported in this study.

CHAPTER FIVE: CONCLUSIONS

The main objective of this research was to investigate the formation of adiabatic shear bands in AISI 4340 steel and explore the possibility of eliminating the damaging effect of adiabatic shear bands in this material by heat treatment procedure. Adiabatic shear bands were formed by subjecting the steel samples in as quenched and tempered condition to rapid deformation by impact using modified Split Hopkinson Pressure Bar (SHPB). The following conclusions can be made from the results of the experimental investigations:

- The shear band deformation in the investigated steel sample is dependent on the strain rates. The higher the strain rate, the shorter is the time for the commencement of stress collapse and strain localization.
- The time and critical strain for commencement of strain localization do not only depend on the strain rates but also on the microstructure of the steel.
- The adiabatic shear bands formed in the steel samples during the impact loading are mostly white etching bands forming a circle when viewed in the transverse section and elliptical shape when viewed in the longitudinal section. In some cases a small fraction of the shear bands in both transverse and longitudinal section are deformed bands.
- In most cases, the adiabatic shear bands form two symmetrical cones with each facing the circular ends of the test specimens. The axis of the cones is parallel to the direction of the applied impact loading.

- The adiabatic shear bands form smooth circles in the samples tempered at 315°C, while they propagate along the wavy (contoured) path in the samples tempered at 425°C.
- Single bands are formed in the samples tempered at 315°C, while double and triple bands are simultaneously initiated and propagated in most of the samples tempered to 425°C.
- The micro hardness measurement showed that the hardness value inside the adiabatic shear band is much higher than in the bulk of the specimen due to the very fine carbides and the high dislocation density inside the shear bands.
- The adiabatic shear bands are a preferred path for crack initiation and propagation which cause the material to fracture into two identical fragments in some test specimens.
- Crack initiation in the adiabatic shear bands occurs by formation of micro-pores which coalesce to form clusters of pores. The clusters are subsequently linked by cracks running parallel to the shear bands. The micro-cracks subsequently transform into full blown cracks leading to sample fragmentation.
- Heat treatment of the adiabatic shear band at 315 °C for two hours does not produce any noticeable change in the structure and hardness of adiabatic shear bands in the impacted steel samples.
- As the tempering temperature is increased from 300 to 600°C for a soaking time of 1 hr, recovery of the pre-impact microstructure and properties in the

shear bands become more pronounced. At 400 °C, no significant change occurs while the change becomes pronounced as the temperature was raised to 500 °C. A considerable change occurs in the shear bands by heat treating at 600 °C for 1 hr.

- Heat treated of the shear bands at 650°C for 20 min. showed a big change in the microstructure and the hardness of shear bands decreases to a value that is slightly higher the original hardness value of the steel sample before impact.
- Complete microstructure and property recovery is obtained by heating the impacted samples at 650°C for 2 hrs. The brittle white adiabatic shear bands are completely replaced with a ductile material whose microstructure is similar in appearance to that of the bulk material.
- The microstructural and property changes occurring in shear bands during high temperature thermal treatment can be traced to nucleation of new grains by coalescence of fine sub-grains in the white etching bands.

REFERENCES

1. C. Zener, J.H Hollomon, Effect of strain rate upon plastic flow of steel, Journal of Applied Physics 15 (1944) 22-32

2. M. A. Meyers, C.L Wittman, The effect of metallurgical parameters on shear band formation in low-carbon (~0.20 Pct) steels, Metal Trans 21A (1990) 3153- 3164.

3. M. N. Bassim, N. Panic, High strain rate effects on the strain of alloy steels, Journal of materials Processing Technology, 92-93 (1999), 481-485.

4. Q. Wei. L. Keckes, T. Jiao, K.T. Hatwig, K.T. Ramesh, E. Ma, Adiabatic shear bands in ultrafine-grained Fe processed by severe plastic deformation, Acta Materialia, 52 (2004) 1859-1869.

5. D.R. Chichili, K.T. Ramesh, K. Hemker, Adiabatic shear localization in α-titanium: experiments, modelling and microstructural evolution, Journal of Mechanics and Physics of Solids, 52 (2004) 1889-1909.

6. L. Qiang, X. Yongbo, M.N. Bassim, Dynamic mechanical properties in relation to adiabatic shear band formation in titanium alloy-Ti117, Materials Science and Engineering A, 358 (2003) 128-133

7. J.R. Li, J.L. Yu, Z.G Wei. Influence of specimen geometry on adiabatic shear instability of tungsten heavy alloys, International Journal of Impact Engineering 28 (2003) 303-314.

8. Y. B. Xu, W. L. Zhong, Y. J. Chen, L. T. Shen, Q. Liu, Y. L. Bai and M. A. Meyers, Shear localization and recrystallization in dynamic deformation of 8090 Al–Li alloy, Materials Science and Engineering A, 299 (2001) 287-295.

9. J. A. Hines and K. S. Vecchio, Recrystallization kinetics within adiabatic shear bands, Acta Materialia, 45 (1997) 635-649.

10. Q. Li', Y. B. Xu, Z. H. Lai, L. T. Shen and Y. L. Bai, Dynamic recrystallization induced by plastic deformation at high strain rate in a Monel alloy, Materials Science and Engineering A, 272 (2000) 250-256.

11. M. T. Pérez-Prado, J. A. Hines and K. S. Vecchio, Microstructural evolution in adiabatic shear bands in Ta and Ta–W alloys, Acta materialia, 49 (2001) 2905-2917.

12. J.X. Li, G.B. Shan, K.W. Gao, L.J. Qiao, W. Y. Chu, In situ SEM study of formation and growth of shear bands and micorcracks in bulk metallic glasses, Materials Science and Engineering A, 354 (2003) 337-343.

13. M. Guden and I. W. Hall, Dynamic properties of metal matrix composites: a comparative study, Material Science and Engineering A, 242 (1998) 141-152.

14. S.E. Schoenfeld, T.W. Wright, A failure criterion based on material instability, International Journal of Solids and Structures, 40 (2003) 3021-3037.

15. J. Barry, G. Bryne, TEM study on the surface white layer in two turned hardened steels, Materials Science and Engineering, A 325 (2002) 356-364.

16. Z.H Chen, L.C. Chan, T. C. lee, C.Y. Tang, An investigation on the formation and propagation of shear band in fine-blanking process, Journal of materials Processing Technology, 138 (2003) 610-614.

17. M.N Raftenber, C.D. Krause, Metallurgical observations of armour steel specimens from plates perforated by shaped charged jets, International Journal of Impact Engineering 23 (1999) 757-770.

18. D.C Erlich, L. Seaman, D.A. Schockey, D.R. Curran, Development and application of a computational shear band model. BRL-CR-00416.

19. P.K Wright, metallurgical effects at high strain rates in the secondary shear zone of the machining operation, in metallurgical effects at high strain rates, edited by Rohde, Butcher, Holland and Karnes, Plenum Press (1973) 547-558.

20. R. C. Glenn and W.C. Leslie: Metallurgical Transactions, vol. 2 (1971) 2945-2947.

21. K-M. Cho, S. Lee, S.R. Nutt, J. Duffy, Adiabatic shear band formations during dynamic torsional deformations of an HY-100 steel, Acta Metal. Mater. 41 (1993) 923-932.

22. J. Duffy and Y. C. Chi, On the measurement of local strain and temperature during the formation of adiabatic shear bands, Material Science and Engineering A, 257 (1992) 195-210.

23. C.L. Wittman, M.A. Meyers, H.R. Pak. Observation of an adiabatic shear band in AISI 4340 steel by high voltage transmission electron microscopy, Metallurgical transaction A, Vol 21A (1990) 707-716.

24. M.A. Meyers, Y.B Xu, Q. Xue, M. T. Perez-Prado, T.R, McNelley Microstructural evolution in adiabatic shear band localization in stainless steel, Acta Materialia 51 (2003) 1307 -1325.

25. J. L. Derep: Microstructure transformation induced by adiabatic shearing in armoured steel, Acta metal. Vol 35, No 6, (1987) 1245-1249.

26. A.K. Zurek: The study of adiabatic shear bands Instability in a pearlitic 4340 steel using a dynamic punch test, Metallurgical and Materials Transactions, vol. 25A (1994) 2483-2489.

27. A. Marchand and J. Duffy, An experimental study of the formation process of adiabatic shear bands in a structural steel, Journal of Mechanics and Physics of Solids, 36 (1988) 251-283.

28. T.W Right and J.W Walter, On stress collapse in adiabatic shear bands, Journal of Mechanics and physics of Solids, 35 (1987) 701-720.

29. T.W. Wright, Steady shearing in a viscoplastic solid, Journal of Mechanics and Physics of Solids 35 (1987) 269-282.

30. H. Feng, and M.N. Bassim, Finite element modelling of the formation of adiabatic shear bands in AISI 4340 steel, Materials Science and Engineering A266 (1999) 255-260.

31. V.F. Nesterenko, M.A. Meyers, T.W. Wright, Self organisation in the initiation of adiabatic shear bands, Acta Materialia 46 (1998) 327-34.

32. D. Peirce, R.J. Asaro, A. Needleman, Material rate dependence and localized deformation in crystalline solids, Acta Metallurgica 31 (1984) 1951-1976.

33. L. Anand, S.R. Kalinidi, The process of shear band formation in plane strain compression of FCC metals: Effects of crystallographic texture, Mechanics of Materials 17 (1994) 223-243.

34. R. W. Armstrong and F. J. Zerilli, Dislocation mechanics aspects of plastic instability and shear banding, Mechanics of Materials 17 (1994) 319-327.

35. G.R. Johnson, W.H. Cook, A constitutive model and data for metals subjected to large strains, high strain rates, and high temperatures, Proceedings of the 7th International Symposium on Ballistics. The Hague (Netherlands); 1983. p. 541–547.

36. L. Daridon, Oussouaddi, S. Ahzi, Influence of the material constituitive models on the adiabatic shear band spacing: MTS, power law and Johnston-Cook models, International Journal od Solids and Structures 41 (2004) 3109 – 3124.

37. R. C. Batra, and L. Chen, Effect of viscoplastic relations on the instability strain, shear band initiation strain, the strain corresponding to the minimum shear band spacing, and the band width in a thermoviscoplastic material, Internal Journal of Plasticity 17 (2001) 1465-1489.

38. A.-S. Bonnet-Lebouvier, A. Molinari, P. Lipinski, Analysis of the dynamic propagation of adiabatic shear bands, International Journal of Solids and Structures 39 (2002) 4249-4269.

39. T.W. Wright, On the speed of an unconstrained shear band in a perfectly plastic material, International Journal of Solids and Structures, 40 (2003) 871-879.

40. Q. Xue, V.F Nesterenko, M.A. Meyers, Evaluation of the collapsing thick-wall cylinder technique for shear-band spacing, International Journal of Impact Engineering 28 (2003) 257-280.

41. Q. Xue, M.A. Meyers, V.F. Nesterenko, Self organisation of shear bands in titanium and Ti-6Al-4V alloy, Acta Materialia 50 (2002) 575-596.

42. D.E. Grady, M.E Kipp, The growth of unstable thermoplastic shear with application to steady-wave shock compression in solids, Journal of Mechanics and Physics of Solids 35 (1987) 95-119.

43. T.W. Wright, H. Ockendon, A scaling law for the effect of inertia on the formation of adiabatic shear bands, International Journal of plasticity 12 (1997) 927-934

44. B. Zhang, W. Shen, Y. Liu, R. Zhang, some factors influencing adiabatic shear banding in impact wear, Wear, 214 (1998) 259-263.

45. Wingrove, Journal of Aust. Institute of Metals, 16 (1971) 67-70.

46. J. Liermann, Dr –Ing. Thesis, WZL-RWTH Aachen, Shaker Verlag, 1988

47. H.K. Tonshoff, D Brandt, H.G. Wobker, SME Technical paper MR 95-215, 1995.

48. H.C Rogers and C. V. Shastry: In Schock Waves and High Strain Rate Phenomena in Metals, M.A Meyers and L.E Murrs, eds, Plenum Press, New York, NY, 1986, p. 285.

49. T. Pintat: In Impact Loading and Dynamic behaviour of materials, C.Y. Chiem, H.-D. Kunze, and L.W. Meyer eds DGM Informations Geselschaft, Federal republic of Germany, 1988, p. 737

50. J.A. Hines, K. S. Vecchio, S. Ahzi, Metallurgical and Materials transactions A, 29 (1998) 191.

51. M. Nabil. Bassim, Study of the formation of adiabatic shear bands in steels, Journal of Materials Processing Technology 119 (2001) 234-236.

52. A Hartley, J. Duffy, R.H. Hawley, Journal of Mechanics and Physics of Solids 35 (1987) 283 -301.

53. U.S Lindholm, G. R. Johnson, Material behaviour under high stress and ultra-high loading rates, J. Mescall and V. Weiss, eds, Plenum Press, New York, 1983, 61-79

54. S.C. Shrivastava, J.J. Jonas, G. Canova, Journal of Mechanics and Physics of Solids 30 (1982) 75

55. R. Nakkalil, J.R. Hornaday Jr. and M. Nabil Bassim, Characterization of the compression properties of rail steels at high temperatures and strain rates, Materials Science and Engineering A 141 (1991) 247-260

56. A. Molinary R.J. Clifton, Analytical characterization of shear localisation in thermoviscoplastic materials, Journal of Applied mechanics 54 (1987) 806-812.

57. T.W. Wright, Approximate analysis for the formation of adiabatic shear bands, Journal of mechanics and Physics of solids 38, 515-30.

58. M.N. Bassim, Effect of specimen geometry in dynamic torsion testing, Experimental Mechanics, Allison (ed.) 1998 Balkema, Rotterdam, 911-913.

59. M. A. Meyers, Dynamic failure: mechanical and microstructural aspects, Journal de Physique III, 6 (1994) C8-597-621

60. J.R. Klepaczko, Behaviour of Ti-6Al-4V alloy at high strain rates, shear testing up to $6*10^4$ l/s and failure criterion, Proc. Conf. DYMAT 2000, J. Phys. IV France 10(2000) 191-196.

61. D.C Erlich, D.R Curran, L. Seaman: Further development of a computational Shear band model, Report AMMRC TR 80-3, SRI International, Menlo park, CA, 1980, 51.

62. H. C. Rogers: Ann Rev. Mater. Sci., 1979, vol. 9, pp. 238-311.

63. H.A. Grebe, H-r. Pak, M.A Meyers: Adiabatic shear band localization in Titanium and Ti Pct Al-4 Pct V alloy, Metallurgical Transactions A 16 (1985) 761-775

64. P. R. Guduru, A. J. Rosakis and G. Ravichandran: Dynamic shear bands: an investigation using high speed optical and infrared diagnostics, Mechanics of Materials 33 (2001) 371-402.

65. J.R. Klepazko, Failure Dynamics: New area of research, Journal de Physique IV, 110 (2003) 615-620.

66. R.S. Culver, in R. W. Rhode, B.M Butcher, J.R Holland and C.H. Karnes (eds.) Metallurgical Effects at High Strain Rates, Plenum, London (1973) 519.

67. A. K. Sinhar, Recovery Recrystallization and Grain Growth, in Ferrous Metallurgy, Butterworths Publishers, Stoneham, USA (1989) 43-76

68. H. Hu, in Metallurgical Treatise, (J.K. Tien and J.F. Elliot, Eds), Conference Proceedings, The Materials Society, AIME, Warrendale, Pa., (1983) 385-407.

69. H. Hu, in L. Himmel (Ed.), Recovery and Recrystallization of Metals, Interscience, New York, 1963, 311.

70. S.B. Davenport, R.L. Higginson, Strain path effects under hot working: an introduction, Journal of materials Processing Technology 98 (200) 267-291

71. M. Jin, A.M. Minor, E.A. Stach, J.W. Morris Jr, Direct observation of deformation-induced grain growth during nano-indentation of ultrafine-grained Al at room temperature, Acta Materialia 52 (2004) 5381-5387

72. H. Paul, J.H. Driver, C. Maurice, Z. Jasienski, Crystallographic aspects of the early stages of recrystallization in brass-type shear bands, Acta Materialia 50 (2002) 4339-4355.